A global simulation of brown carbon: Implications for photochemistry and direct radiative effect

D. S. Jo[1], R. J. Park[1,*], S. Lee[1], S.-W. Kim[1], and X. Zhang[2]

[1]{School of Earth and Environmental Science, Seoul National University, Seoul, 151-747, Republic of Korea}

[2]{Department of Civil and Environmental Engineering, University of California, Davis, CA, USA}

Correspondence to: R. J. Park (rjpark@snu.ac.kr)

Abstract

Recent observations suggest that a certain fraction of organic carbon (OC) aerosol effectively absorbs solar radiation, which is also known as brown carbon (BrC) aerosol. Despite much observational evidence of its presence, very few global modeling studies have been conducted because of poor understanding of global BrC emissions. Here we present an explicit global simulation of BrC in a global 3-D chemical transport model (GEOS-Chem), including global BrC emission estimates from primary (3.9 ± 1.7 and 3.0 ± 1.3 TgC yr^{-1} from biomass burning and biofuel) and secondary (5.7 TgC yr^{-1} from aromatic oxidation) sources. We evaluate the model by comparing the results with observed absorption by water-soluble OC in surface air in the United States, and with single scattering albedo observations at AERONET sites all over the globe. The model successfully reproduces the seasonal variations of observed light absorption by water-soluble OC, but underestimates the magnitudes, especially in regions with high secondary source contributions. Our global simulations show that BrC accounts for 21% of the global mean surface OC concentration, which is typically assumed to be scattering. We find that the global direct radiative effect of BrC is nearly zero at the top of the atmosphere, and consequently decreases the direct radiative cooling effect of OC by 16%. In addition, the BrC absorption leads to a general reduction of NO_2 photolysis rates, whose maximum decreases occur in Asia up to -8% (-17%) on an annual (spring) mean basis. The resulting decreases of annual (spring) mean surface ozone concentrations are up to -6% (-13%) in Asia, indicating a non-negligible effect of BrC on photochemistry in this region.

47 ## 1 Introduction

48 Carbonaceous aerosols (CAs) are one of the poorly understood aerosols (Goldstein
49 and Galbally, 2007; Park et al., 2003) and are divided into black carbon (BC) and organic
50 carbon (OC) aerosols. These two types of CAs are emitted together mainly by combustion
51 processes (except for secondary organic carbon, SOC). In the literature, BC is considered as
52 light-absorbing and OC as light-scattering aerosols until recently. Therefore, the climatic
53 effect of CAs depends on the relative contributions of BC to CAs. For example, the net direct
54 radiative forcing (DRF) of biomass burning is estimated to be negligible, whereas diesel use
55 causes climate warming although the first source is larger than the latter for CAs (Forster et
56 al., 2007).

57 Many field observations and chamber studies recently showed that a certain fraction
58 of OC could absorb solar radiation, especially for ultra-violet wavelengths (< 400 nm)
59 (Alexander et al., 2008; Hecobian et al., 2010; Kirchstetter and Thatcher, 2012; Kirchstetter
60 et al., 2004; Yang et al., 2009). This light-absorbing OC fraction is referred to as brown
61 carbon (BrC) aerosol (Andreae and Gelencser, 2006; Laskin et al., 2015). If BrC is prevalent,
62 and its DRF is significant, then previous estimates of the DRF of CAs need to be revised.

63 Recent studies showed that the solar absorption of BrC is not negligible, and is even
64 comparable to that of BC (Alexander et al., 2008; Chung et al., 2012; Kirchstetter and
65 Thatcher, 2012). Using residential wood smoke samples, Kirchstetter and Thatcher (2012)
66 calculated that BrC absorption accounts for 14% of total solar absorption by CA, and even
67 contributes 49% of solar absorption of CA at wavelengths below 400 nm. Chung et al. (2012)
68 found that OC contributes about 45% of CA absorption at 520 nm by analyzing observations
69 at the Gosan site in South Korea. Using aerosol optical property observations at Aerosol

70 Robotic Network (AERONET) sites, Bahadur et al. (2012) estimated that BrC absorption at
71 440 nm is about 40% of BC absorption at the same wavelength, whereas at 675 nm it is less
72 than 10% of BC absorption.
73 Several efforts have also been made to examine the chemical and physical properties
74 of BrC. Some studies showed that humic-like substances (HULIS) were related to BrC
75 (Hoffer et al., 2006; Kim and Paulson, 2013; Lukács et al., 2007) based on the high
76 absorption Ångström exponent (AAE) of HULIS in the range of 6–7, indicating that the
77 specific absorption increases substantially towards the shorter wavelengths (Hoffer et al.,
78 2006), although the sources and the dominating chromophores of HULIS have not clearly
79 been revealed yet (Moise et al., 2015; Graber and Rudich, 2006). Alexander et al. (2008)
80 observed individual BrC spheres in East Asian outflows, and showed that the characteristics
81 of BrC spheres (AAE of 1.5) were different from those of HULIS and also strongly
82 absorbing. On the other hand, several classes of compounds have been identified as potential
83 contributions to BrC - nitroaromatic compounds, such as nitrophenols, imidazole-based and
84 other N-heterocyclic compounds, and quinones (Laskin et al., 2015). Furthermore, SOC
85 produced from aromatic species has been found to absorb solar radiation, especially in high
86 NOx conditions (Jaoui et al., 2008; Laskin et al., 2015; Lin et al., 2015; Liu et al., 2012;
87 Nakayama et al., 2010; Nakayama et al., 2013; Yu et al., 2014; Zhong and Jang, 2011).
88 Even though the chemical composition of BrC is not clearly understood yet,
89 observations strongly indicate possible important sources of BrC (Laskin et al., 2015). Using
90 the positive matrix factorization analysis of absorption at 365 nm over the southeastern
91 United States in 2007, Hecobian et al. (2010) showed that biomass burning was the most
92 dominant source of BrC (55%), followed by SOC (26-34%). Many other studies have also

93 suggested biomass burning as the most important BrC source (Chakrabarty et al., 2010;
94 Clarke et al., 2007; Favez et al., 2009; Hoffer et al., 2006; Kirchstetter and Thatcher, 2012;
95 Kirchstetter et al., 2004; McMeeking, 2008; Saleh et al., 2014). Several studies recently
96 proposed SOC as an additional BrC source, especially when it is aged in the atmosphere
97 (Bones et al., 2010; Flores et al., 2014; Hawkins et al., 2014; Jaoui et al., 2008; Laskin et al.,
98 2014; Laskin et al., 2010; Liu et al., 2014; Nakayama et al., 2010; Nakayama et al., 2013;
99 Nguyen et al., 2012; Updyke et al., 2012; Zhang et al., 2011; Zhong and Jang, 2011).
100 Despite the ample observational studies, very few modeling studies have been
101 conducted to simulate global and regional distributions of BrC and to further quantify its
102 radiative effect (Feng et al., 2013; Jacobson, 2001; Lin et al., 2014; Park et al., 2010; Wang et
103 al., 2014). Jacobson (2001) first assumed 10% of OC as a solar-absorbing aerosol in a model,
104 and this assumption resulted in an increase of the global DRF by 0.03–0.05 W m^{-2}. Park et al.
105 (2010) estimated BrC concentrations in East Asia using the mass ratio of BrC to BC, and the
106 resulting annual clear-sky DRF of BrC over East Asia was 0.05 W m^{-2}. Feng et al. (2013)
107 simulated global BrC concentrations by considering 92% of OC from biomass burning and
108 biofuel use as BrC, and estimated 0.09 W m^{-2} for the global clear-sky DRF of BrC. Lin et al.
109 (2014) calculated the DRF of OC by assuming that all of the biomass burning and the biofuel
110 OC is BrC, and all of the SOC (as a high-absorbing case) as BrC. They estimated the global
111 clear-sky DRF of OC as -0.20 W m^{-2}.
112 In this study, we estimate global primary BrC emissions from open burning and
113 biofuel use based on a reported relationship between AAE and modified combustion
114 efficiency (MCE) (McMeeking, 2008). In addition to the primary source above, we also
115 consider SOC produced from aromatic oxidation as a secondary source of BrC (Hecobian et

al., 2010; Jaoui et al., 2008; Lin et al., 2015; Nakayama et al., 2010; Nakayama et al., 2013; Zhong and Jang, 2011). Based on these sources, a global distribution of BrC concentrations is explicitly simulated for the entire year of 2007 using a global 3-D chemical transport model (GEOS-Chem). We evaluate the model by comparing its results with observations in the United States and all over the globe. Using the best estimate of annual mean BrC concentrations, we examine the global direct radiative effect (DRE) of BrC and its effect on photochemistry.

2 BrC emissions

In this section, we discuss our method to estimate primary and secondary sources of BrC, and provide explicit global BrC emissions. The primary and secondary sources include biomass burning and biofuel use, and the production from aromatic volatile organic compounds (VOCs), respectively. Estimated global emissions are used as input for GEOS-Chem below to explicitly simulate spatial and temporal distributions of BrC concentrations.

2.1 Primary sources

Biomass burning is the largest source of CA aerosols globally (Bond et al., 2004). OC is primarily emitted during the smoldering (low-temperature burning) phase of combustion (Chakrabarty et al., 2010; Chakrabarty et al., 2014; Schnaiter et al., 2006), whereas BC is preferentially emitted from the flaming (high-temperature burning) phase. Therefore, BrC is also emitted largely during the smoldering phase of burning. Here we use the relationship between the burning efficiency and the observed aerosol light absorption to estimate the BrC emission from biomass burning.

Previous studies have suggested MCE defined in Eq. (1) below to provide

quantitative information of burning efficiencies that can be categorized into flaming versus smoldering combustion (Kaufman et al., 1998; Ward et al., 1992; Ward and Hao, 1991). For example, Reid et al. (2005) used a MCE value of 0.9 to differentiate between flaming (MCE > 0.9) and smoldering combustion (MCE < 0.9).

$$\mathrm{MCE} = \frac{\Delta C_{CO_2}}{\Delta C_{CO_2} + \Delta C_{CO}}, \quad (1)$$

where ΔC is the change in species concentration in fire off-gas relative to clean air [molecules m^{-3}].

McMeeking (2008) further found a linear relationship between the observed attenuation Ångström exponents and the calculated MCE values from a number of biomass burning samples, as shown in Eq. (2).

$$\mathring{A} = -17.34 \times \mathrm{MCE} + 18.20, \quad (2)$$

where Å is the AAE of biomass burning samples.

The coefficient of determination (R^2) of the relationship in Eq. (2) is 0.39, so the associated uncertainty appears to be significant. However, the negative relationship between AAE and MCE in Eq. (2) is robust as identified by previous studies (Saleh et al., 2014; Kirchstetter and Thatcher, 2012). For example, absorption of aerosols from biomass burning can be contributed by either BC or BrC, or both (Moise et al., 2015). As discussed above, the absorption of carbonaceous aerosols is mainly caused by BC at high MCE conditions (>0.9); in contrast, the BC/CA ratio is almost zero at low MCE conditions (<0.8) (McMeeking, 2008). Using Eq. (2), we calculate AAE values of 0.86 and 4.3 at MCE values of 1.0 and 0.8, respectively, and each calculated AAE is in good agreement with the observed BC (0.86) and BrC AAE (5.0) from biomass burning samples measured by Kirchstetter and Thatcher (2012).

Saleh et al. (2015) also showed that the BC to OC ratio (proportional to MCE) has negative relationship with AAE.

In addition, we are able to obtain the BrC/BC absorption ratio using AAE. In Appendix A, we present a detailed description of our method for estimating the relationship between the BrC/BC absorption ratio and AAE. Our method assumes external mixing, and this assumption can cause uncertainties when particles are internally mixed (such as coating effect). For uncertainty analysis, we calculate three BrC/BC absorption cases as shown in Figure 1, which shows the estimated BrC/BC absorption ratio at 550 nm as a function of MCE. Different lines indicate different AAEs of BC and BrC according to the Table 1 of Kirchstetter and Thatcher (2012). They calculated BC AAE and BrC AAE using 115 wood smoke samples. For the calculation of BrC AAE, BC AAE had to be decided, and they assumed three different BC AAEs (0.86, 1.00, 1.15) based on their smoke samples and previous studies. Resulting BrC AAEs were 5.00, 5.48, and 6.19. We conduct three simulations according to the Figure 1, as described later in this section. For high MCE conditions (>0.95), the BrC contribution to the CA absorption is negligible, whereas it becomes significant for low MCE conditions (<0.85).

We calculate the MCE of biomass burning based on the Fire Inventory from NCAR (FINN) (Wiedinmyer et al., 2011) with vegetation dependent emission factors of CO_2 and CO using Eq. (3) as follows:

$$\mathrm{MCE} = \frac{\Delta C_{CO_2}}{\Delta C_{CO_2} + \Delta C_{CO}} = \frac{EF_{CO_2}/MW_{CO_2}}{EF_{CO_2}/MW_{CO_2} + EF_{CO}/MW_{CO}}, \quad (3)$$

where EF is the emission factor [g-species kg-dry matter^{-1}] and MW is the molecular weight [g-species mole^{-1}].

183 Finally, mass absorption efficiency (MAE), which is used for converting light
184 absorption to mass concentration, is needed to obtain the BrC/BC mass ratio from the
185 BrC/BC absorption ratio. For the fresh BC MAE at 550 nm, we use the value of 7.5 $m^2 g^{-1}$
186 recommended by Bond and Bergstrom (2006) (Nakayama et al., 2013; Park et al., 2010). For
187 BrC, a large range of MAE values (0.09-4.1 $m^2 g^{-1}$ at 550 ± 30 nm) has been reported
188 (Alexander et al., 2008; Cheng et al., 2011; Chung et al., 2012; Clarke et al., 2007; Favez et
189 al., 2009; Hecobian et al., 2010; Hoffer et al., 2006; Kirchstetter et al., 2004; McMeeking,
190 2008; Yang et al., 2009). The highest MAE (3.6-4.1 $m^2 g^{-1}$ at 550 nm) was observed by
191 Alexander et al. (2008), who used transmission electron microscopy to identify the optical
192 properties of individual BrC particles in the atmosphere. Generally, low MAEs were reported
193 when analyzing water soluble organic carbon (WSOC) from water extracts (Cheng et al.,
194 2011; Hecobian et al., 2010; Srinivas and Sarin, 2014), indicating that WSOC may include
195 both BrC and colorless OC. Intermediate MAEs mostly came from optical measurements
196 (Chung et al., 2012; Favez et al., 2009; Yang et al., 2009). For the primary BrC MAE, we use
197 1.0 $m^2 g^{-1}$ at 550 nm based on McMeeking (2008), who conducted a number of MAE
198 measurements of biomass burning samples (~30 unique fuels tested in ~230 burns) using both
199 filter-based and optical-based methods. In brief, we use the MAE values of 7.5 $m^2 g^{-1}$ and 1.0
200 $m^2 g^{-1}$ at 550 nm for BC and primary BrC, respectively. But at a shorter wavelength, higher
201 MAE value was used for primary BrC (e.g., 5.3 $m^2 g^{-1}$ at 365 nm as discussed in Section 4).
202 Using the results in Figure 1 with Eq. (3), we calculate the EF (mass) ratio of BrC to
203 OC as summarized in Table 1. The EF ratio of BrC to OC differs for each vegetation type and
204 assumed BC AAE (0.86-1.15). Among different vegetation types, cropland burning shows the
205 highest BrC to OC mass ratio, driven by the low MCE and the highest ratio of BC to OC EF.

206 Because we calculate the BrC to OC EF ratio by multiplying the BrC to BC EF ratio by the
207 BC to OC ratio, the high BC to OC ratio can lead to a high BrC to OC ratio. Although Table 1
208 shows the highest BrC/OC ratio from cropland burning, its contribution to the global BrC
209 emission is small because the OC emission from the cropland is the lowest (Wiedinmyer et
210 al., 2011). Instead, the tropical forest burning is the highest, and the resulting total BrC
211 emission from biomass burning is 3.9 ± 1.7 TgC yr^{-1}, which contributes about 17 ± 7% of
212 total OC emission from biomass burning (22.7 TgC yr^{-1}) (Wiedinmyer et al., 2011).
213 Our method of estimating BrC emissions from biofuel use is similar to that of
214 estimating emissions from biomass burning. We estimate BrC/OC ratio using the MCE and
215 BC to OC ratio in the same way as the biomass burning estimates. The only difference is that
216 the biofuel emission of each sector is not known (the biomass burning emission is known for
217 each vegetation type). Therefore, we first estimate OC biofuel emissions from each biofuel
218 category with the information given by previous studies (Bond et al., 2007; Bond et al., 2004;
219 Fernandes et al., 2007). Because there is no clear evidence that BrC is emitted by dung,
220 charcoal, and the industrial sector, here we consider only fuelwood and agricultural residue as
221 BrC sources. Fuelwood burning is the largest contributor to biofuel BrC emission. Our
222 estimate of BrC/OC mass ratio is 0.271 - 0.663 from biofuel use. Overall results are
223 summarized in Table 2. Note that base year of Table 2 is 2000 because previous studies
224 reported their values based on 2000. We scale up the emission for 2007 as described in
225 Section 3.2. Resulting BrC emission from biofuel use is 3.0 ± 1.3 TgC yr^{-1}, which is
226 comparable to BrC emission from biomass burning.

227 **2.2 Secondary source**

228 We consider SOC as a source of BrC in the model based on the observed optical

229 characteristic of SOC, depending on its chemical formation, as follows: 1) anthropogenic
230 (aromatic) SOCs tend to absorb solar radiation more efficiently than biogenic SOCs
231 (Jacobson, 1999; Nakayama et al., 2010; Zhong and Jang, 2011; Zhong et al., 2012); 2) the
232 solar absorption efficiency increases as SOCs undergo atmospheric aging processes (Bones et
233 al., 2010; Lambe et al., 2013; Laskin et al., 2015; Laskin et al., 2010; Updyke et al., 2012); 3)
234 SOCs formed in inorganic seeds have a darker color than others (Jaoui et al., 2008;
235 Nakayama et al., 2013; Zhong and Jang, 2011; Zhong et al., 2012); moreover, SOCs become
236 darker when they undergo aging in the presence of nitrogen-containing inorganic gases and
237 aerosols (Bones et al., 2010; Laskin et al., 2010; Liu et al., 2012).
238 Among those factors, the first two are more important than the last. For example, the
239 absorbance of aged biogenic SOCs produced in inorganic seeds is much lower than that of
240 fresh anthropogenic SOCs under no-seed conditions (Zhong and Jang, 2011). Furthermore,
241 Lambe et al. (2013) suggested that the effect of NOx on SOC light absorption is small under
242 typical ranges of VOC/NOx. Therefore, here we consider the first two factors for BrC
243 simulations in the model. We assume anthropogenic (aromatic) SOCs with high atmospheric
244 aging as BrC in the model. Atmospheric aging is calculated using the volatility basis set
245 (VBS) approach with six bins in the model (Jo et al., 2013), where SOC concentrations of the
246 first two bins are considered as BrC. However, we note that some brown SOCs can be
247 bleached when they undergo photodissociation (Zhong and Jang, 2011; Sareen et al., 2013).
248 Furthermore, browning reactions can be accelerated by cloud and fog processing of aerosols
249 (Moise et al., 2015), which are not considered in this study. More detailed treatments of the
250 chemical aging of BrC are needed in future BrC models.
251 BrC from anthropogenic SOC has different optical properties (i.e, MAE, imaginary

refractive index) compared with BrC from wood burning. Therefore, we apply different optical parameters for the model evaluation (Section 4) such as 5.3 $m^2 g^{-1}$ (McMeeking, 2008) for primary BrC and 1.5 $m^2 g^{-1}$ (Nakayama et al., 2010) for secondary BrC at 365 nm (note that the MAE of primary BrC at 550 nm is 1.0 $m^2 g^{-1}$ as discussed in Section 2.1). The estimated annual source of secondary BrC is 5.7 TgC yr^{-1}, which contributes 45% of total BrC sources.

3 Model description

3.1 General

We use the GEOS-Chem (version 9.1.2) global 3-D chemical transport model (Bey et al., 2001) to simulate BrC for 2007. The model is driven by Modern Era Retrospective-analysis for Research and Applications (MERRA) assimilated meteorological data from the Global Modeling and Assimilation Office Goddard Earth Observing System (Rienecker et al., 2011). The data include winds, precipitation, temperature, boundary layer height, and other meteorological variables at 0.5° × 0.667° horizontal resolutions, but are degraded to 2° × 2.5° for computational efficiency.

We conduct a fully coupled oxidant-aerosol simulation, including SO_4^{2-} - NO_3^- - NH_4^+, soil dust, and sea salt aerosols. The simulation of carbonaceous aerosols in the GEOS-Chem is based on Park et al. (2003; 2006). The model carries BC and POC, with a hydrophobic and hydrophilic fraction for each. We assume that 80% of BC and 50% of POC are emitted as hydrophobic (the rest is hydrophilic), then hydrophobic aerosols become hydrophilic with an e-folding time of 1.15 days (Cooke et al., 1999). For the SOC simulation, we use the VBS approach based on Jo et al. (2013). All SOC is considered as hydrophilic,

and more details are described in previous SOC studies (Chung and Seinfeld, 2002; Henze and Seinfeld, 2006; Henze et al., 2008; Jo et al., 2013; Liao et al., 2007). Note that we consider only the carbon mass of OC including BrC as discussed below, to avoid uncertainties involved in converting organic carbon to organic matter concentrations, which is typically done by multiplying a constant ratio (e.g, 1.4-2.1) (Aiken et al., 2008; Turpin and Lim, 2001).

3.2 Emissions

We use fossil fuel and biofuel emissions of CAs for 2000 with no monthly variations from Bond et al. (2007). However, domestic wood burning for heating has strong seasonal dependency, so we additionally use the Monitoring Atmospheric Composition & Climate/City Zen (MACCity) emission inventory (Diehl et al., 2012; Granier et al., 2011) to obtain seasonal variations of global biofuel emissions and to scale up for 2007. For this, we divide the whole globe into regions with similar seasonality according to the Atmospheric Chemistry and Climate Model Intercomparison Project (ACCMIP) (Lamarque et al., 2010), which is the basis of the MACCity inventory. We apply the annual trend of each ACCMIP region to the emissions from Bond et al. (2007). The emissions for each region and trends are listed in Table S1 and Table S2.

We use biomass burning emissions from FINN version 1.0 (Wiedinmyer et al., 2011), which provides global daily estimates of trace gases and aerosols at 1 km horizontal resolution for 2002-2012 (http://bai.acd.ucar.edu/Data/fire/). However, the FINN version 1.0 inventory does not include aromatic VOCs (benzene, toluene, and xylene), the emissions of which are estimated by multiplying dry burned matter by emission factors from Akagi et al. (2011) and Andreae and Merlet (2001).

4 Model Evaluation

We conduct a model evaluation using the observed light absorption of WSOC measured by Hecobian et al. (2010) and Zhang et al. (2011; 2013) in the United States. The model evaluation allows us not only to validate simulated BrC concentrations but also to examine each source contribution to BrC in the United States. We also use the global single scattering albedo (SSA) observations from the AERONET to evaluate the effect of including BrC on light absorption by aerosols over the globe.

4.1 United States

Prior to evaluating BrC simulations, we first focus on BC and OC aerosols in the model to examine the general model performance in simulating carbonaceous aerosol concentrations in the United States. We use BC and OC observations from the Interagency Monitoring of Protected Visual Environments (IMPROVE) network for 2007 (Malm et al., 1994). Most sites were situated in rural regions, measuring background concentrations of BC and OC. The data were available every three days; more than 20,000 samples were used for our comparison. For comparison with the model results, we computed the observed monthly mean concentrations of BC and OC averaged on the 2°×2.5° model grid.

Figure 2 shows scatterplot comparisons of the observed and simulated monthly mean BC and OC concentrations in the United States. The model slightly underestimates both BC and OC over the United States, consistent with similar comparisons in Huang et al. (2013). We calculate the annual mean concentrations of the model using the simulated values of model grid boxes corresponding to the IMPROVE network sites. The simulated annual mean BC concentration is 0.22 μgC m^{-3}, which is 12% lower than the observed mean value (0.25 μgC m^{-3}). However, the bias in the model is larger for OC by 30% (1.16 and 0.81 μgC m^{-3} for

observed and simulated OC concentrations, respectively), which is additionally due to the underestimation of SOC in the model (Jo et al., 2013). This low bias for SOC can be reflected in the simulated BrC concentrations, which is discussed later in this section.

We use the light absorption observations of WSOC measured using a UV-Vis spectrophotometer and Long-Path absorption Cell by Hecobian et al. (2010), and compare them with the light absorption by BrC in the model. Absorption coefficients of WSOC at 365 nm were measured at 15 sites in the southeastern United States in 2007. Among them, eight sites are in urban areas, and the others are in rural regions. Detailed descriptions of the measurements are available in Hecobian et al. (2010).

Because light absorption observations are measured only for water soluble fractions of OC, and do not include water insoluble components, we separate BrC in the model into water soluble and water insoluble components. The model divides OC (or BrC) into hydrophilic and hydrophobic components. For the comparison, we do not use the simulated hydrophilic fraction, but instead use an observed WSOC/OC ratio because the assumed division of hydrophobic and hydrophilic fractions of OC and their conversion can be applicable in a global sense, but in a regional sense, it may cause a significant discrepancy. For example, the observed water soluble fraction of the total OC is generally low (on the order of 25%) in the Los Angeles basin (Zhang et al., 2013), on the other hand, the model simulates a high water-soluble fraction of the total OC (63-74%) in this region. For this reason, we decide to use the observed WSOC/OC ratio for the evaluations. In the southeastern United States, the observed WSOC/OC ratio is about 0.58 (Weber et al., 2007; Zhang et al., 2013), which is also used to estimate the water soluble BrC concentrations from the total BrC concentrations in the model.

Because the model simulates a mass concentration of BrC, a conversion from the mass concentration to light absorption is carried out by multiplying MAE values. For BrC from wood burning, we use the MAE value of 5.3 m^2 g^{-1} at 365 nm measured by McMeeking (2008) in order to retain the consistency between our emission estimates and the evaluation. For BrC from SOC, we select the MAE of 1.5 m^2 g^{-1} at 365 nm calculated by Nakayama et al. (2010) (see Figure 4 in their paper).

Figure 3 shows monthly mean simulated and observed light absorption coefficients of BrC at 365 nm averaged over all sites in the southeastern United States for 2007. Black circles and colored bars indicate the observed and simulated BrC absorption at 365 nm, respectively, and different colors in the bar show contributions from different sources. Each panel represents different model simulations with each case for AAE selections as shown in Figure 1 and Table 1.

In winter months (November through March), the observed light absorptions were generally high and reached a peak in March. These high absorptions were highly correlated with levoglucosan, which is a marker for biomass burning (Hecobian et al., 2010). During the summer, the observed light absorptions decreased substantially.

The model generally captures the observed seasonal variation with high absorption in the winter, having a peak in March and low absorption in the summer (R of 0.93). On an annual mean basis, we find that the model is too high by 46% for case 1, and is too low by -31% for case 3, relative to the observations, respectively. The model for case 2 is in the best agreement with the observations (4%) on an annual mean basis.

The BrC source contribution in the model is similar to the observed source contribution. Hecobian et al. (2010) showed that biomass burning was the main contributor

for the winter season, whereas the SOC contribution increased during the summer season. The simulated seasonal variation is consistent with the observation, as shown in Figure 3. The annual mass contribution of SOC to BrC is 38% (in case 2), which is in good agreement with the observed contribution of 32% (Hecobian et al., 2010). Based on the results in Figure 3, the model for the case 2 yields best estimates of BrC emissions.

In addition to the observation by Hecobian et al. (2010), we use the light absorption observations by Zhang et al. (2011; 2013). Measurements were carried out in Atlanta, GA (33.778427N, 84.396181W), Pasadena, CA (34.140528N, 118.122455W), and Riverside, CA (33.97185N, 117.32266W) for a month or less. As discussed above, we apply the observed WSOC/OC ratio to the model BrC concentrations: 26% for the Los Angeles basin (Pasadena and Riverside) (Zhang et al., 2013) and 58% for Atlanta (Weber et al., 2007; Zhang et al., 2013).

Figure 4 shows the daily mean observed and simulated light absorption coefficients from the best model (case 2) for Atlanta, Pasadena, and Riverside for 2010. The upper panel shows the comparison of the observed versus simulated light absorption for Atlanta. The highest observed daily absorption occurred on August 24, but the model fails to reproduce it. Furthermore, the model generally overestimates the observed absorption by 44%, and the large discrepancies mainly occur in September. This large discrepancy in September is similar to the result shown in Figure 3(b) for 2007.

The middle and lower panels show the comparisons at the Los Angeles basin sites in May and June. The observed mean light absorptions at these sites (0.81 and 0.98 Mm^{-1} for Pasadena and Riverside, respectively) are higher than the observed mean light absorption (0.56 Mm^{-1}) for Atlanta. However, the model underestimates the observations by 38%

(Pasadena) and 48% (Riverside). Zhang et al. (2013) showed that the main sources of BrC at these sites were SOC from anthropogenic emissions. The model also shows a high contribution (85%) of the secondary source to the total BrC mass concentrations, but the magnitudes are generally lower than the observations, and this low bias is likely related to underestimation of the simulated SOC concentrations using the 1-D VBS (Jo et al., 2013).

We find from the model evaluation over the United States that the model generally captures the observed mean absorption and its seasonal variability in the region where primary sources are dominant. On the other hand, the model underestimates the observed mean absorption in the region with the dominant secondary sources. The low bias is partly explained by the SOC underestimation in the model. However, the underestimations of BrC from SOC (38-48%) are higher than those of SOC (18%), indicating the importance of additional secondary BrC sources that we did not include in the model.

A MAE value for secondary BrC could be another possible reason for the bias in the model. Although chamber studies suggested weak absorbing characteristics of BrC from SOC (Nakayama et al., 2010; Nakayama et al., 2013; Zhong and Jang, 2011), some field observations speculated the existence of strongly-absorbing BrC from SOC (Alexander et al., 2008; Chung et al., 2012). For example, applying the MAE value of 3.5 m^2 g^{-1} at 365 nm (a half of the MAE at 365 nm from Alexander et al. (2008)) for secondary BrC yields a similar mean absorption value to the observation over LA basin. Extensive observations of optical characteristics of BrC depending on the formation mechanisms would be needed to reduce the associated uncertainties and to improve the model.

4.2 Evaluation against global AERONET observations

No global observation of BrC is available yet. Here we use the observed SSA at

AERONET sites to evaluate the model by focusing on the effect of BrC on the simulated aerosol absorption. We also use observed aerosol optical depth (AOD) to evaluate the model capability to simulate aerosol mass concentrations.

For comparisons of AOD and SSA between the model and observations, we use FlexAOD (http://pumpkin.aquila.infn.it/flexaod/), which calculates AOD and SSA using simulated aerosol mass concentrations from GEOS-Chem with the Mie algorithm (Mischenko et al., 2002; Curci et al., 2015).

For optical properties of BrC, we use imaginary refractive indices of BrC from McMeeking (2008) for wood burning sources, and from Nakayama et al. (2010) for SOC sources. Detailed description of the values used in AOD and SSA calculation are provided in Section 6, where we discuss the DRE of BrC.

Figure 5 shows comparisons of monthly mean simulated versus observed AOD at 500 nm and SSA at 440 nm. We find that the model captures the observed AOD quite well with a regression slope of 0.86 and a R of 0.88. However, the model tends to overestimate the observed SSA, implying that the simulated aerosol concentrations appear to have too large a fraction of scattering aerosols. We find that the inclusion of BrC in the model reduces the high bias of simulated SSA by 33% and 23% (lower left and lower right panel of Figure 5), indicating a considerable contribution of BrC to aerosol absorption. Although the statistics suggest a greater improvement with the case 1 in terms of the bias, simulated SSA values at sites in Africa with high BrC concentrations, are too low apart from the regression line (discrepancy > 0.1). This result also supports our selection of the case 2 as the best model for BrC emission estimates.

Despite a decrease of simulated SSA with BrC, the model is still too high relative to

436 the observations. The overestimation might be partly caused by the underestimation of BC
437 emissions from biomass burning (Bond et al., 2013). This is also supported by the fact that
438 the discrepancy gets larger for biomass burning regions, where a difference between the
439 model and AERONET SSA is 40% higher than that in regions with high anthropogenic
440 emissions. Emission factors of BC used in this study are 0.2-0.69 g kg^{-1} (Wiedinmyer et al.,
441 2011), which are lower than the value of 1 g kg^{-1} used by Chin et al. (2009), who found no
442 significant bias in their model compared with the AERONET SSA. Lin et al. (2014) also
443 reported a small bias in their model compared with AERONET SSA using 4.7 Tg yr^{-1} of
444 global annual biomass burning BC emissions, which is about two times higher than 2.2 Tg yr^{-1}
445 of this study.
446 In addition to the biomass burning emission of BC, the anthropogenic emission of BC
447 could also contribute to the simulated SSA bias. Cohen and Wang (2014) showed that a
448 global top-down emission of BC is twice as large as the bottom-up estimates of BC based on
449 the Kalman Filter approach. They suggested that BC emissions in East Asia, Southeast Asia,
450 and Eastern Europe are significantly underestimated in current bottom-up emission
451 inventories. This issue is critically important, and possibly has an important implication for
452 climate. However, an investigation of BC emissions for the SSA discrepancy above is beyond
453 the scope of our work, and will be conducted in future studies.
454 Light absorption enhancement of aged BC could also be one of the reasons for the
455 SSA overestimation in the model. Here we use the same optical parameters for all BC in the
456 model. However, Bond et al. (2006) suggested that the absorption of aged BC is about 1.5
457 times greater than that of fresh BC. BC aging occurs as it is mixed internally with other
458 aerosols. If we assume hydrophilic BC as aged BC in the model and its absorption

enhancement by a factor of 1.5 relative to hydrophobic BC, the high bias of simulated SSA is additionally reduced by about 20% (not shown).

We further compare the model against AERONET AAE as shown in Figure S1. We find that the model overestimates the observed AAE after including BrC, in part, because the model underestimates BC emissions as discussed above. However, the simulated AAE will be decreased if we increase BC emissions as suggested by the top-down estimate (Cohen and Wang, 2014). For example, for regions (North America, Central America, South America, Southeast Asia, and Australia) where the difference between our BC emission and the top-down estimate is within a factor of 2, we find that the model with BrC shows a better agreement with the observed AAE (Figure S2) and with the observed SSA (Figure S3).

Considering all these uncertainties, our evaluation above indicates that the model for the case 2 results in the best estimates of simulated BrC concentrations, which will be used for examining BrC effects on climate and photochemistry, below and other two cases are considered as upper and lower limits of our estimates.

5 Global budgets

5.1 Annual surface concentration

Figure 6 shows our best estimates of annual mean concentrations of BrC and each source contribution in surface air for 2007. Values are high in regions where biomass burning (Southeast Asia and South America) and biofuel (East Asia and Northeast India) sources are dominant. These primary sources account for 77% of BrC concentrations in surface air. On the other hand, secondary sources are relatively minor in the surface, but their contribution increases in the free troposphere, as discussed in Section 5.2.

Figure 7 shows BrC to BC and OC ratios in surface air in the model. The BrC to BC ratio is highest over the eastern North Pacific and the North Atlantic. This high ratio over the ocean reflects a secondary chemical production, which contributes to BrC but not to BC. Over the continents, the ratio is generally higher in heavy biomass burning regions (South America and Africa) than in industrialized regions (East Asia, Europe, and the eastern United States) because more BrC than BC is emitted from biomass burning.

Similarly, the BrC to OC ratio is also high over the oceans because of secondary BrC, the concentrations of which increase with atmospheric aging. Over the continents, the ratio is smaller reflecting relatively fresh emissions of OC from anthropogenic sources that do not directly contribute to BrC. We find that the BrC to OC ratio is relatively high in regions with large biofuel use (North India and Central Asia). Although China is one of the largest emission source regions for BrC (Figure 6), both BrC to BC and BrC to OC ratios are relatively low because of high concentrations of BC and OC. Our global mean BrC to BC and BrC to OC ratios at the surface are 1.24 and 0.21, respectively and are lower than the ratio (3.4 of BrC to BC ratio and 0.43 of BrC to OC ratio in terms of burden) of Feng et al. (2013), but higher than the ratio (1.0 of BrC to BC ratio) used in Park et al. (2010).

5.2 Tropospheric budget of BrC

Table 3 summarizes our best estimates of the global tropospheric budgets of BrC, along with BC and OC. The global BrC source is 12.5 ± 3.0 TgC yr^{-1}, which accounts for 27% of OC sources. Although the biofuel emission (6.5 TgC yr^{-1}) is three times lower than the biomass burning emission (22.7 TgC yr^{-1}) for OC, the biofuel emission (3.0 ± 1.3 TgC yr^{-1}) becomes significant for BrC, contributing about 43% of primary sources. The secondary source of BrC is 5.7 TgC yr^{-1}, and is comparable to the primary sources (6.8 ± 3.0 TgC yr^{-1}).

505 Wet deposition is the main removal process for BrC, and accounts for 86 % of total
506 removal processes. The remaining loss is due to dry deposition. The contribution of wet
507 deposition to total deposition of BrC is similar to that of OC (82%), because we treat BrC
508 scavenging similarly to that of OC. Because secondary BrC is produced all over the
509 troposphere (not only at the surface) and is hydrophilic, most secondary BrC is removed by
510 wet deposition processes (92%).
511 The global burden of BrC shows the highest contribution from secondary BrC (50 %)
512 compared to primary contributions from biomass burning (30 %) and biofuel (20 %). This
513 result is opposite to the source contributions in surface air shown in Figure 6. The
514 contribution of secondary BrC to the atmospheric burden is twice as high as the contribution
515 of secondary BrC to the surface concentration (23%), reflecting a relatively large production
516 of BrC in the free troposphere as well as limited export of primary BrC from the surface to
517 the free troposphere.
518 Our BrC lifetime is 5.8 days, which is lower than that of OC (7.9 days) because of
519 different contributions of the secondary sources for BrC and OC. The latter species includes a
520 larger fraction of secondary species (52%), the lifetime of which is usually longer than that of
521 POC especially for not aged biogenic SOC (Jo et al., 2013). No significant difference
522 between the lifetimes of BrC and BC exists because BrC, which is more hydrophilic than BC,
523 is more prone to wet scavenging than BC.
524
525 **6 Direct radiative effect of BrC**
526 We use imaginary refractive indices of BrC as a function of wavelength for radiative
527 transfer calculations to account for the wavelength dependency of the BrC absorption.

Imaginary refractive indices in the literature have a wide range of values, even from the same sources, such as wood burning (Chakrabarty et al., 2010; Kirchstetter et al., 2004; McMeeking, 2008). In order to maintain the consistency with BrC emission estimates from primary sources, we use the imaginary refractive indices reported by McMeeking (2008), which are 0.18, 0.14, and 0.10 at 370, 405, and 532 nm, respectively. The values are interpolated with the AAE at every 50 nm wavelength interval for the radiative transfer calculations. For secondary BrC, values from Nakayama et al. (2010) are used with 0.047 and 0.007 at 355 and 532 nm, respectively, based on the measurements for SOC from toluene.

We calculate AOD, SSA, and asymmetry parameter using FlexAOD, which is described in Section 4.2. Note that we calculate DRE rather than DRF. DRE is the instantaneous radiative impact of all atmospheric particles on the Earth's energy balance, and DRF is the change in DRE from pre-industrial to present-day (Heald et al., 2014). We use the Rapid Radiative Transfer Model for GCMs (RRTMG) (Iacono et al., 2008) for DRE calculations. Wavelengths used for the calculation are 300, 304, 393, 533, 702, 1010, 1270, 1462, 1784, 2046, 2325, 2788, 3462, and 8021 nm. MERRA reanalysis data are used for albedo and other meteorological variables.

Figures 8(a) and 8(b) show the clear sky DRE values of primary and secondary BrC concentrations. Because the imaginary refractive indices of BrC are between those of strongly absorbing BC and scattering OC, the global mean DRE of BrC is close to zero, as shown in (a) and (b).

Although the DRE of BrC at the top of the atmosphere is nearly zero, the increased DRE of OC after considering BrC absorption (usually considered as scattering OC) is 0.11 W m^{-2}, as shown in Figure 8(c). The DRE of OC without BrC absorption is -0.69 W m^{-2} (Figure

551 8(d)), and this value is increased to -0.58 W m^{-2} after considering BrC absorption.
552 Consequently, the cooling effect of OC is reduced by 16%.
553 Despite the negligible effect of BrC on DRE or DRF, its significance manifests for
554 OC DRF estimates, which have been conducted based on the assumption of scattering OC.
555 For example, AeroCom phase II simulations calculated -0.03 W m^{-2} as the global mean DRF
556 of POC from fossil fuel and biofuel, and -0.06 W m^{-2} for that of SOC (Myhre et al., 2013).
557 Because the biofuel emission is about twice as large as the fossil fuel emission (Bond et al.,
558 2007), and one-half of OC from biofuel is BrC, one-third of the POC from fossil fuel and
559 biofuel is BrC. Therefore, one-third of DRF (-0.01 W m^{-2}) of POC in AeroCom is related to
560 BrC, whose DRF is close to zero. For SOC, because the pre-industrial biogenic SOC
561 concentration is similar to present-day conditions, almost all DRF of SOC is from
562 anthropogenic SOC. Based on previous SOC studies (Henze et al., 2008; Jo et al., 2013;
563 Murphy and Pandis, 2010), approximately one-third of anthropogenic SOC is highly aged,
564 and can thus be assumed to be BrC in this simple estimation. As a result, one-third of DRF (-
565 0.02 W m^{-2}) of SOC in AeroCom is related to BrC. The total DRF of BrC that was assumed
566 to be scattering OC in the AeroCom study is -0.03 W m^{-2}. Because DRF of BrC is almost
567 negligible, the negative DRF of OC (-0.09 W m^{-2}) in AeroCom could likely be overestimated
568 by 50%. We think, however, the warming effect of BrC on the negative DRF or DRE of OC
569 would be a low-end value because our best model likely underestimates BrC concentrations
570 especially from the secondary source.
571
572 **7 Effect on ozone photochemistry**
573 BrC absorption, particularly at UV wavelengths, has an important implication for

574 ozone photochemistry. Here we examine the effect of BrC absorption on photochemistry by
575 updating photolysis rate calculations in GEOS-Chem following Martin et al. (2003). Table 4
576 shows the calculated extinction efficiency and SSA of important aerosols at 0.4 μm, which
577 affect UV extinction, and thus photolysis rate calculations, in the model. Values of OC, BC, and
578 inorganic aerosols are from GEOS-Chem, in which we update aerosol optical properties by
579 adding those of BrC. We include optical properties of primary and secondary BrC separately
580 because they differ substantially. For example, SSA values of primary BrC are smaller than
581 those of secondary BrC, and thus have a greater impact on UV radiation. Compared with
582 other aerosols, SSA values of BrC are generally lower than those of OC and inorganic
583 aerosols, but higher than those of BC.
584 Martin et al. (2003) showed that the effects of aerosols on photolysis rates increased
585 CO by 5-15 ppbv in the remote Northern Hemisphere (annual mean concentrations less than
586 140 ppbv). This increase resulted in an improved model agreement with observations, but
587 there was a still gap between the model and the observations. In our simulation with BrC, CO
588 concentration is further increased by 0.2-1.9 ppbv in remote Northern Hemisphere regions
589 (annual mean concentrations less than 140 ppbv in the model). On the other hand, OH
590 concentrations are decreased by 0-10% in the boundary layer over the Northern Hemisphere
591 (maximum decreases occur in regions with high BrC concentrations, shown in Figure 6). The
592 change of OH owing to BrC is about one-third of the OH change according to the overall
593 aerosol effects from Martin et al. (2003). Therefore, the inclusion of BrC significantly affects
594 tropospheric chemistry, especially for regions with heavy biomass burning and biofuel
595 emissions.
596 Finally, we quantify the effects of BrC on global NO_2 photolysis rates and ozone

597 concentrations at the surface. Figure 9 shows changes in annual NO_2 photolysis rates and O_3
598 concentrations in surface air owing to BrC absorption. Although BrC absorption is included,
599 there are no significant changes (less than 1%) of the global mean NO_2 photolysis rate and O_3
600 concentration in surface air. However, the effect of BrC appears to be important for regions
601 with high BrC concentrations. We find a maximum decrease of the annual mean NO_2
602 photolysis rate by 8% in surface air over Asia where the resulting reduction of O_3
603 concentration is up to -2 ppbv (6% of annual mean surface O_3 concentration). We also find
604 that the BrC effect has a strong seasonal variation such that it is maximized in the spring
605 when surface O_3 concentration is decreased up to -13% in Asia because of high BrC
606 concentration (55 μgC m^{-3}). This maximum O_3 decrease by BrC (-13%) is similar to the O_3
607 decrease (15%) by fire aerosols in Jiang et al. (2012).
608
609 **8 Conclusion**
610 OC has been considered to be a scattering aerosol, but emerging evidence has shown
611 that some OC can efficiently absorb solar radiation. This absorbing OC is called BrC. With
612 increasing recognition of its importance, especially for solar absorption at UV and short
613 visible wavelengths, quantification of its spatial and temporal distribution is much needed for
614 the study of climate and air quality issues. Here we conducted an explicit global BrC
615 simulation for the full year of 2007 using a global 3-D chemical transport model (GEOS-
616 Chem), and examined its implication for climate and O_3 photochemistry.
617 We first estimated primary BrC emissions from biomass burning and biofuel use
618 based on the relationship between AAE and MCE. Our estimates of primary BrC emissions
619 are 3.9 ± 1.7 and 3.0 ± 1.3 TgC yr^{-1} from biomass burning and biofuel use, respectively. The

620 secondary BrC source is estimated to be 5.7 TgC yr^{-1} from the aromatic oxidation.

621 With explicit BrC emissions, a coupled oxidant-aerosol simulation was conducted for
622 2007 to obtain the spatial and temporal distributions of BrC concentrations. We first
623 evaluated the model by comparing the simulated versus observed BrC absorption in the
624 United States and found that the model successfully reproduced the observed seasonal
625 variation of light absorption by WSOC in the southeastern United States, whereas the model
626 significantly underestimated secondary BrC over the Los Angeles basin.

627 Our budget analysis showed that BrC from primary sources are dominant (77%) in
628 surface air, but BrC from secondary sources becomes important with increasing altitudes. For
629 example, BrC from secondary sources accounts for the 50% of the tropospheric BrC burden,
630 which is higher than its 23% contribution to surface BrC concentrations. Our global mean
631 value of the BrC to BC ratio is 1.83 for the whole atmosphere, and 1.24 for the surface, which
632 significantly differs from the values used in previous studies.

633 Using our best results, we estimated the DRE of BrC to be close to zero at the top of
634 the atmosphere because the imaginary refractive indices of BrC are in the midpoint between
635 those of BC and OC. Despite a negligible contribution to DRE, the inclusion of BrC
636 absorption in the model offsets the negative radiative effect of OC by 0.11 W m^{-2} (16%).

637 Finally, we included BrC absorption in photolysis rate calculations in the model. We
638 found that the NO_2 photolysis rate is decreased up to 8%, especially for Asia, where BrC
639 concentration is high. Resulting annual surface O_3 concentrations are decreased up to -2 ppbv
640 (6%). This effect is more important in the spring, when a typical O_3 maximum occurs in Asia,
641 where the effect of BrC decreases the surface O_3 concentration by up to -13%.

642 Many chemical transport models and air quality models have included the effect of

aerosols on photolysis rate calculations, but have not considered the BrC effect. Based on our analysis, BrC absorption could have a significant direct impact on regional air quality by being involved in O_3 photochemical formation. Its significance, however, can be expanded to the globe by its effect on the atmospheric oxidation capacity, which has an indirect but important implication for global air quality and climate.

Appendix A

A1 Relationship between BrC/BC absorption ratio and AAE

In this section we describe a procedure for obtaining the relationship between the BrC/BC absorption ratio and AAE. Assuming no internal mixing and dust influence, total absorption at a certain wavelength (λ) can be expressed as:

$$\alpha_{\lambda,CA} = \alpha_{\lambda,BrC} + \alpha_{\lambda,BC} \quad \text{(A1)}$$

Rewriting Eq. (A1) using AAE:

$$\alpha_{\lambda_0,CA}\left(\frac{\lambda}{\lambda_0}\right)^{-\overset{O}{A}_{CA}} = \alpha_{\lambda_0,BrC}\left(\frac{\lambda}{\lambda_0}\right)^{-\overset{O}{A}_{BrC}} + \alpha_{\lambda_0,BC}\left(\frac{\lambda}{\lambda_0}\right)^{-\overset{O}{A}_{BC}} \quad \text{(A2)}$$

Dividing each side of Eq. (A2) by $\alpha_{\lambda_0,BC}$:

$$(1+F)\left(\frac{\lambda}{\lambda_0}\right)^{-\overset{O}{A}_{CA}} = F\left(\frac{\lambda}{\lambda_0}\right)^{-\overset{O}{A}_{BrC}} + \left(\frac{\lambda}{\lambda_0}\right)^{-\overset{O}{A}_{BC}} \quad \text{(A3)}$$

where F is the BrC/BC absorption ratio at λ_0.

We can solve Eq. (A3) analytically, and the procedure is described in Appendix A2. We do not use the analytical relationship because it uses only three wavelengths for the calculations. The Ångström relationship is based on empirical fitting. AAE varies in different wavelength regions, even if we use the same samples. For example, Chung et al. (2012)

showed that CA AAE is about 1.2 when the first four wavelengths (370, 470, 520, 590 nm) are used, while the CA AAE is 1.35 with the last four wavelengths (590, 660, 880, 950 nm). This discrepancy is much increased in the case of BrC AAE. Liu et al. (2014) showed that BrC AAE varies by approximately 20%, depending on wavelength pairs. Furthermore, if we calculate AAE of BrC using the MAE of Kirchstetter et al. (2004), AAE of BrC in all wavelengths (from 350 to 650 nm, 7 values) is fitted to 5.9 with a R^2 of 0.96. However, the AAE of BrC using just two wavelengths is 4.1 for the 350-440 nm and 8.0 for the 550-600 nm, respectively.

Therefore, we calculate the relationship between MCE and F by regression using multiple wavelengths: [300, 350, 400, 450, 500, 550, 600, 650, 700, 750, 800, 850, 900 nm]. If we rewrite Eq. (A3) for the regression form,

$$\overset{\circ}{\text{A}}_{\text{CA}} \log(\lambda) + \text{C} = -\log\left[\text{F}\left(\frac{\lambda}{\lambda_0}\right)^{-\overset{\circ}{\text{A}}_{\text{BrC}}} + \left(\frac{\lambda}{\lambda_0}\right)^{-\overset{\circ}{\text{A}}_{\text{BC}}} \right] \quad \text{(A4)}$$

where the residual term C is

$$\text{C} = -\overset{\circ}{\text{A}}_{\text{CA}} \log(\lambda_0) - \log(1 + \text{F}) \quad \text{(A5)}$$

The left side of Eq. (A4) has the shape of Ax+B. Therefore, by linear regression analysis, we can obtain Å_{CA} (the slope of the regression) as varying F on the right side. For example, Figure S4 shows the linear regression case for F=4.0. In this case, R^2 is 0.99 and Angstrom exponent of CA is 4.44. Y-intercept of the numerical fitting is -29.81, which is consistent with Y-intercept (-29.64) from Eq. (A5). The difference between two Y-intercept values are always within 1%, which shows the numerical fitting with Eq. (A4) satisfies both the slope (A) and the intercept (B) at the same time within 1% error. We choose an Å_{BrC} values of {5.0, 5.48,

685 6.19} and an $Å_{BC}$ values of {0.86, 1.00, 1.15}, following Kirchstetter and Thatcher (2012),
686 who estimated mean $Å_{BrC}$ using several wood samples (87 samples) over the 360 to 700 nm
687 spectrum range. We assign a λ_0 value of 550 nm. The coefficient of determination (R^2) is
688 greater than 0.98 in all the regression analyses. The calculated relationship between MCE and
689 F is plotted in Figure 1. As expected, emissions of BrC are increased when MCE is
690 decreased.
691

692 **A2 Analytical derivation of Eq. (A3)**

693 Here we describe the procedure to obtain the analytical relationship between MCE
694 and F. First, substituting λ_1 and λ_2 in Eq. (A3),

695 $$(1+F)\left(\frac{\lambda_1}{\lambda_0}\right)^{-Å_{CA}} = F\left(\frac{\lambda_1}{\lambda_0}\right)^{-Å_{BrC}} + \left(\frac{\lambda_1}{\lambda_0}\right)^{-Å_{BC}} \quad \text{(A6)}$$

696 $$(1+F)\left(\frac{\lambda_2}{\lambda_0}\right)^{-Å_{CA}} = F\left(\frac{\lambda_2}{\lambda_0}\right)^{-Å_{BrC}} + \left(\frac{\lambda_2}{\lambda_0}\right)^{-Å_{BC}} \quad \text{(A7)}$$

697 Assuming AAE between λ_0 and λ_1 is equal to AAE between λ_0 and λ_2, divide Eq. (A6) by Eq.
698 (A7), and rearrange terms:

699 $$\left(\frac{\lambda_1}{\lambda_2}\right)^{-Å_{CA}} = \frac{F\left(\frac{\lambda_1}{\lambda_0}\right)^{-Å_{BrC}} + \left(\frac{\lambda_1}{\lambda_0}\right)^{-Å_{BC}}}{F\left(\frac{\lambda_2}{\lambda_0}\right)^{-Å_{BrC}} + \left(\frac{\lambda_2}{\lambda_0}\right)^{-Å_{BC}}} \quad \text{(A8)}$$

700 Taking the logarithm of both sides:

701 $$\overset{o}{A}_{CA} = -\log\left(\frac{F\left(\frac{\lambda_1}{\lambda_0}\right)^{-\overset{o}{A}_{BrC}} + \left(\frac{\lambda_1}{\lambda_0}\right)^{-\overset{o}{A}_{BC}}}{F\left(\frac{\lambda_2}{\lambda_0}\right)^{-\overset{o}{A}_{BrC}} + \left(\frac{\lambda_2}{\lambda_0}\right)^{-\overset{o}{A}_{BC}}}\right) / \log\left(\frac{\lambda_1}{\lambda_2}\right) \quad \text{(A9)}$$

702 Substituting Eq. (2) into Eq. (A9) gives:

703 $$\text{MCE} = \left[18.2 + \log\left(\frac{F\left(\frac{\lambda_1}{\lambda_0}\right)^{-\overset{o}{A}_{BrC}} + \left(\frac{\lambda_1}{\lambda_0}\right)^{-\overset{o}{A}_{BC}}}{F\left(\frac{\lambda_2}{\lambda_0}\right)^{-\overset{o}{A}_{BrC}} + \left(\frac{\lambda_2}{\lambda_0}\right)^{-\overset{o}{A}_{BC}}}\right) / \log\left(\frac{\lambda_1}{\lambda_2}\right)\right] / 17.34 \quad \text{(A10)}$$

704 After assigning $\mathring{A}_{BrC}$, $\mathring{A}_{BC}$, and the corresponding three wavelengths (λ_0, λ_1 and λ_2) in Eq.

705 (A10), we obtain the relationship between MCE and F analytically.

706

707 **Acknowledgements**

708 This study was supported by the Eco Innovation Program of KEITI (ARQ201204015) and by

709 Korea Ministry of Environment as "Climate Change Correspondence Program".

710

711

712

713

714

715

716

717

718

References

Aiken, A. C., DeCarlo, P. F., Kroll, J. H., Worsnop, D. R., Huffman, J. A., Docherty, K. S., Ulbrich, I. M., Mohr, C., Kimmel, J. R., and Sueper, D.: O/C and OM/OC ratios of primary, secondary, and ambient organic aerosols with high-resolution time-of-flight aerosol mass spectrometry, Environmental Science & Technology, 42, 4478-4485, 2008.

Akagi, S., Yokelson, R., Wiedinmyer, C., Alvarado, M., Reid, J., Karl, T., Crounse, J., and Wennberg, P.: Emission factors for open and domestic biomass burning for use in atmospheric models, Atmospheric Chemistry and Physics, 11, 4039-4072, 2011.

Alexander, D. T. L., Crozier, P. A., and Anderson, J. R.: Brown carbon spheres in East Asian outflow and their optical properties, Science, 321, 833, 2008.

Andreae, M. and Gelencser, A.: Black carbon or brown carbon? The nature of light-absorbing carbonaceous aerosols, Atmospheric Chemistry and Physics, 6, 3131-3148, 2006.

Andreae, M. O. and Merlet, P.: Emission of trace gases and aerosols from biomass burning, Global Biogeochemical Cycles, 15, 955-966, 2001.

Bahadur, R., Praveen, P. S., Xu, Y., and Ramanathan, V.: Solar absorption by elemental and brown carbon determined from spectral observations, Proceedings of the National Academy of Sciences, 109, 17366-17371, 2012.

Bey, I., Jacob, D. J., Yantosca, R. M., and Logan, J. A.: Global modeling of tropospheric chemistry with assimilated meteorology- Model description and evaluation, Journal of Geophysical Research, 106, 073-023,095, 2001.

Bond, T. C. and Bergstrom, R. W.: Light absorption by carbonaceous particles: An investigative review, Aerosol Science and Technology, 40, 27-67, 2006.

Bond, T. C., Bhardwaj, E., Dong, R., Jogani, R., Jung, S., Roden, C., Streets, D. G., and Trautmann, N. M.: Historical emissions of black and organic carbon aerosol from energy-related combustion, 1850-2000, Global Biogeochemical Cycles, 21, 2007.

Bond, T. C., Doherty, S. J., Fahey, D. W., Forster, P. M., Berntsen, T., DeAngelo, B. J., Flanner, M. G., Ghan, S., Kärcher, B., Koch, D., Kinne, S., Kondo, Y., Quinn, P. K., Sarofim,

747 M. C., Schultz, M. G., Schulz, M., Venkataraman, C., Zhang, H., Zhang, S., Bellouin, N.,
748 Guttikunda, S. K., Hopke, P. K., Jacobson, M. Z., Kaiser, J. W., Klimont, Z., Lohmann, U.,
749 Schwarz, J. P., Shindell, D., Storelvmo, T., Warren, S. G., and Zender, C. S.: Bounding the
750 role of black carbon in the climate system: A scientific assessment, Journal of Geophysical
751 Research, doi: 10.1002/jgrd.50171, 2013. n/a-n/a, 2013.

752 Bond, T. C., Habib, G., and Bergstrom, R. W.: Limitations in the enhancement of visible light
753 absorption due to mixing state, Journal of Geophysical Research: Atmospheres (1984–2012),
754 111, 2006.

755 Bond, T. C., Streets, D. G., Yarber, K. F., Nelson, S. M., Woo, J. H., and Klimont, Z.: A
756 technology-based global inventory of black and organic carbon emissions from combustion,
757 Journal of Geophysical Research, 109, 14203, 2004.

758 Bones, D. L., Henricksen, D. K., Mang, S. A., Gonsior, M., Bateman, A. P., Nguyen, T. B.,
759 Cooper, W. J., and Nizkorodov, S. A.: Appearance of strong absorbers and fluorophores in
760 limonene-O3 secondary organic aerosol due to NH4+-mediated chemical aging over long
761 time scales, Journal of Geophysical Research, 115, D05203, 2010.

762 Chakrabarty, R., Moosmüller, H., Chen, L. W. A., Lewis, K., Arnott, W., Mazzoleni, C.,
763 Dubey, M., Wold, C., Hao, W., and Kreidenweis, S.: Brown carbon in tar balls from
764 smoldering biomass combustion, Atmospheric Chemistry and Physics, 10, 6363-6370, 2010.

765 Chakrabarty, R. K., Pervez, S., Chow, J. C., Watson, J. G., Dewangan, S., Robles, J., and
766 Tian, G.: Funeral pyres in South Asia: Brown carbon aerosol emissions and climate impacts,
767 Environmental Science & Technology Letters, 1, 44-48, 2014.

768 Cheng, Y., He, K. B., Zheng, M., Duan, F. K., Du, Z. Y., Ma, Y. L., Tan, J. H., Yang, F. M.,
769 Liu, J. M., and Zhang, X. L.: Mass absorption efficiency of elemental carbon and water-
770 soluble organic carbon in Beijing, China, Atmospheric Chemistry and Physics, 11, 11497-
771 11510, 2011.

772 Chin, M., Diehl, T., Dubovik, O., Eck, T., Holben, B., Sinyuk, A., and Streets, D.: Light
773 absorption by pollution, dust, and biomass burning aerosols: a global model study and
774 evaluation with AERONET measurements, Annales Geophysicae, 27, 3439-3464, 2009.

775 Chung, C., Kim, S. W., Lee, M., Yoon, S. C., and Lee, S.: Carbonaceous aerosol AAE

776 inferred from in-situ aerosol measurements at the Gosan ABC super site, and the implications
777 for brown carbon aerosol, Atmospheric Chemistry and Physics, 12, 6173-6184, 2012.

778 Chung, S. and Seinfeld, J.: Global distribution and climate forcing of carbonaceous aerosols,
779 Journal of Geophysical Research, 107, 4407, 2002.

780 Clarke, A., McNaughton, C., Kapustin, V., Shinozuka, Y., Howell, S., Dibb, J., Zhou, J.,
781 Anderson, B., Brekhovskikh, V., and Turner, H.: Biomass burning and pollution aerosol over
782 North America: Organic components and their influence on spectral optical properties and
783 humidification response, Journal of Geophysical Research, 112, D12S18, 2007.

784 Cohen, J. B. and Wang, C.: Estimating global black carbon emissions using a top-down
785 Kalman Filter approach, Journal of Geophysical Research: Atmospheres, 119, 307-323, 2014.

786 Cooke, W., Liousse, C., Cachier, H., and Feichter, J.: Construction of a 1 x 1 fossil fuel
787 emission data set for carbonaceous aerosol and implementation and radiative impact in the
788 ECHAM4 model, Journal of Geophysical Research, 104, 22137-22162, 1999.

789 Curci, G., Hogrefe, C., Bianconi, R., Im, U., Balzarini, A., Baró, R., Brunner, D., Forkel, R.,
790 Giordano, L., Hirtl, M., Honzak, L., Jiménez-Guerrero, P., Knote, C., Langer, M., Makar, P.
791 A., Pirovano, G., Pérez, J. L., San José, R., Syrakov, D., Tuccella, P., Werhahn, J., Wolke, R.,
792 Žabkar, R., Zhang, J., and Galmarini, S.: Uncertainties of simulated aerosol optical properties
793 induced by assumptions on aerosol physical and chemical properties: An AQMEII-2
794 perspective, Atmospheric Environment, 115, 541-552, 2015.

795 Diehl, T., Heil, A., Chin, M., Pan, X., Streets, D., Schultz, M., and Kinne, S.: Anthropogenic,
796 biomass burning, and volcanic emissions of black carbon, organic carbon, and SO2 from
797 1980 to 2010 for hindcast model experiments, Atmospheric Chemistry and Physics
798 Discussions, 12, 24895-24954, 2012.

799 Favez, O., Alfaro, S. C., Sciare, J., Cachier, H., and Abdelwahab, M. M.: Ambient
800 measurements of light-absorption by agricultural waste burning organic aerosols, Journal of
801 Aerosol Science, 40, 613-620, 2009.

802 Feng, Y., Ramanathan, V., and Kotamarthi, V.: Brown carbon: a significant atmospheric
803 absorber of solar radiation?, Atmospheric Chemistry and Physics, 13, 8607-8621, 2013.

804 Fernandes, S. D., Trautmann, N. M., Streets, D. G., Roden, C. A., and Bond, T. C.: Global
805 biofuel use, 1850–2000, Global Biogeochemical Cycles, 21, GB2019, 2007.

806 Flores, J. M., Washenfelder, R., Adler, G., Lee, H., Segev, L., Laskin, J., Laskin, A.,
807 Nizkorodov, S., Brown, S., and Rudich, Y.: Complex refractive indices in the near-ultraviolet
808 spectral region of biogenic secondary organic aerosol aged with ammonia, Physical
809 Chemistry Chemical Physics, 16, 10629-10642, 2014.

810 Forster, P., V. , Ramaswamy, P., Artaxo, T., Berntsen, R., Betts, D. W., Fahey, J., Haywood, J.,
811 Lean, D. C., Lowe, G., Myhre, J., Nganga, R., Prinn, G., Raga, M. S., and Dorland, R. V.:
812 Changes in Atmospheric Constituents and in Radiative Forcing., Cambridge University Press,
813 United Kingdom and New York, NY, USA., 2007.

814 Goldstein, A. H. and Galbally, I. E.: Known and unexplored organic constituents in the earth's
815 atmosphere, Environmental Science & Technology, 41, 1514-1521, 2007.

816 Graber, E. and Rudich, Y.: Atmospheric HULIS: How humic-like are they? A comprehensive
817 and critical review, Atmospheric Chemistry and Physics, 6, 729-753, 2006.

818 Granier, C., Bessagnet, B., Bond, T., D'Angiola, A., Denier van der Gon, H., Frost, G. J.,
819 Heil, A., Kaiser, J. W., Kinne, S., and Klimont, Z.: Evolution of anthropogenic and biomass
820 burning emissions of air pollutants at global and regional scales during the 1980–2010 period,
821 Climatic Change, 109, 163-190, 2011.

822 Hawkins, L. N., Baril, M. J., Sedehi, N., Galloway, M. M., De Haan, D. O., Schill, G. P., and
823 Tolbert, M. A.: Formation of Semisolid, Oligomerized Aqueous SOA: Lab Simulations of
824 Cloud Processing, Environmental science & technology, 48, 2273-2280, 2014.

825 Heald, C., Ridley, D., Kroll, J., Barrett, S., Cady-Pereira, K., Alvarado, M., and Holmes, C.:
826 Contrasting the direct radiative effect and direct radiative forcing of aerosols, Atmospheric
827 Chemistry and Physics, 14, 5513-5527, 2014.

828 Hecobian, A., Zhang, X., Zheng, M., Frank, N., Edgerton, E., and Weber, R.: Water-Soluble
829 Organic Aerosol material and the light-absorption characteristics of aqueous extracts
830 measured over the Southeastern United States, Atmospheric Chemistry and Physics, 10,
831 5965-5977, 2010.

832 Henze, D. K. and Seinfeld, J. H.: Global secondary organic aerosol from isoprene oxidation,

833 Geophysical Research Letters, 33, 09812, 2006.

834 Henze, D. K., Seinfeld, J. H., Ng, N. L., Kroll, J. H., Jacob, D. J., and Heald, C. L.: Global
835 modeling of secondary organic aerosol formation from aromatic hydrocarbons: high-vs. low-
836 yield pathways, Atmospheric Chemistry and Physics, 8, 2405-2420, 2008.

837 Hoffer, A., Gelencsér, A., Guyon, P., Kiss, G., Schmid, O., Frank, G., Artaxo, P., and Andreae,
838 M.: Optical properties of humic-like substances (HULIS) in biomass-burning aerosols,
839 Atmospheric Chemistry and Physics, 6, 3563-3570, 2006.

840 Huang, Y., Wu, S., Dubey, M., and French, N.: Impact of aging mechanism on model
841 simulated carbonaceous aerosols, Atmospheric Chemistry and Physics, 13, 6329-6343, 2013.

842 Iacono, M. J., Delamere, J. S., Mlawer, E. J., Shephard, M. W., Clough, S. A., and Collins, W.
843 D.: Radiative forcing by long-lived greenhouse gases: Calculations with the AER radiative
844 transfer models, Journal of Geophysical Research: Atmospheres (1984–2012), 113, 2008.

845 Jacobson, M. Z.: Global direct radiative forcing due to multicomponent anthropogenic and
846 natural aerosols, Journal of Geophysical Research, 106, 1551-1568, 2001.

847 Jacobson, M. Z.: Isolating nitrated and aromatic aerosols and nitrated aromatic gases as
848 sources of ultraviolet light absorption, Journal of Geophysical Research, 104, 3527-3542,
849 1999.

850 Jaoui, M., Edney, E. O., Kleindienst, T. E., Lewandowski, M., Offenberg, J. H., Surratt, J. D.,
851 and Seinfeld, J. H.: Formation of secondary organic aerosol from irradiated ¥á-
852 pinene/toluene/NOx mixtures and the effect of isoprene and sulfur dioxide, Journal of
853 Geophysical Research, 113, D09303, 2008.

854 Jiang, X., Wiedinmyer, C., and Carlton, A. G.: Aerosols from fires: An examination of the
855 effects on ozone photochemistry in the Western United States, Environmental science &
856 technology, 46, 11878-11886, 2012.

857 Jo, D., Park, R., Kim, M., and Spracklen, D.: Effects of chemical aging on global secondary
858 organic aerosol using the volatility basis set approach, Atmospheric Environment, 81, 230-
859 244, 2013.

860 Kaufman, Y. J., Justice, C. O., Flynn, L. P., Kendall, J. D., Prins, E. M., Giglio, L., Ward, D.

E., Menzel, W. P., and Setzer, A. W.: Potential global fire monitoring from EOS-MODIS, Journal of Geophysical Research, 103, 32215-32238, 1998.

Kim, H. and Paulson, S. E.: Real refractive indices and volatility of secondary organic aerosol generated from photooxidation and ozonolysis of limonene, α-pinene and toluene, Atmos. Chem. Phys., 13, 7711–7723, doi:10.5194/acp-13-7711-2013, 2013.

Kirchstetter, T. and Thatcher, T.: Contribution of organic carbon to wood smoke particulate matter absorption of solar radiation, Atmospheric Chemistry and Physics, 12, 6067-6072, 2012.

Kirchstetter, T. W., Novakov, T., and Hobbs, P. V.: Evidence that the spectral dependence of light absorption by aerosols is affected by organic carbon, Journal of Geophysical Research, 109, D21208, 2004.

Lamarque, J., Bond, T., Eyring, V., Granier, C., Heil, A., Klimont, Z., Lee, D., Mieville, A., and Owen, B.: Historical(1850-2000) gridded anthropogenic and biomass burning emissions of reactive gases and aerosols: methodology and application, Atmospheric Chemistry and Physics, 10, 7017-7039, 2010.

Lambe, A. T., Cappa, C. D., Massoli, P., Onasch, T., Forestieri, S. D., Martin, A. T., Cummings, M. J., Croasdale, D. R., Brune, B., and Worsnop, D. R.: Relationship between oxidation level and optical properties of secondary organic aerosol, Environmental science & technology, 47, 6349-6357, 2013.

Laskin, A., Laskin, J., and Nizkorodov, S. A.: Chemistry of Atmospheric Brown Carbon, Chemical reviews, 115, 4335-4382, 2015.

Laskin, J., Laskin, A., Nizkorodov, S. A., Roach, P., Eckert, P., Gilles, M. K., Wang, B., Lee, H. J., and Hu, Q.: Molecular Selectivity of Brown Carbon Chromophores, Environmental science & technology, 48, 12047-12055, 2014.

Laskin, J., Laskin, A., Roach, P. J., Slysz, G. W., Anderson, G. A., Nizkorodov, S. A., Bones, D. L., and Nguyen, L. Q.: High-resolution desorption electrospray ionization mass spectrometry for chemical characterization of organic aerosols, Analytical chemistry, 82, 2048-2058, 2010.

Liao, H., Henze, D., Seinfeld, J., Wu, S., and Mickley, L.: Biogenic secondary organic

aerosol over the United States: Comparison of climatological simulations with observations, Journal of Geophysical Research, 112, D06201, 2007.

Lin, G., Penner, J. E., Flanner, M. G., Sillman, S., Xu, L., and Zhou, C.: Radiative forcing of organic aerosol in the atmosphere and on snow: Effects of SOA and brown carbon, Journal of Geophysical Research: Atmospheres, 119, 7453-7476, 2014.

Lin, P., Liu, J., Shilling, J. E., Kathmann, S. M., Laskin, J., and Laskin, A.: Molecular characterization of brown carbon (BrC) chromophores in secondary organic aerosol generated from photo-oxidation of toluene, Physical Chemistry Chemical Physics, 2015. 2015.

Liu, J., Scheuer, E., Dibb, J., Ziemba, L. D., Thornhill, K., Anderson, B. E., Wisthaler, A., Mikoviny, T., Devi, J. J., and Bergin, M.: Brown carbon in the continental troposphere, Geophysical Research Letters, 41, 2191-2195, 2014.

Liu, S., Shilling, J. E., Song, C., Hiranuma, N., Zaveri, R. A., and Russell, L. M.: Hydrolysis of organonitrate functional groups in aerosol particles, Aerosol Science and Technology, 46, 1359-1369, 2012.

Lukács, H., Gelencsér, A., Hammer, S., Puxbaum, H., Pio, C., Legrand, M., Kasper-Giebl, A., Handler, M., Limbeck, A., and Simpson, D.: Seasonal trends and possible sources of brown carbon based on 2-year aerosol measurements at six sites in Europe, Journal of Geophysical Research, 112, 2007.

Malm, W. C., Sisler, J. F., Huffman, D., Eldred, R. A., and Cahill, T. A.: Spatial and seasonal trends in particle concentration and optical extinction in the United States, Journal of Geophysical Research, 99, 1347-1370, 1994.

Martin, R. V., Jacob, D. J., Yantosca, R. M., Chin, M., and Ginoux, P.: Global and regional decreases in tropospheric oxidants from photochemical effects of aerosols, Journal of Geophysical Research, 108, 4097, 2003.

McMeeking, G. R.: The Optical, Chemical, And Physical Properties Of Aerosols And Gases Emitted By The Laboratory Combustion Of Wildland Fuels, Dissertation, Department of Atmospheric Science, Colorado State University, Fort Collins, Colorado Fall 2008. Available at: http://chem.atmos.colostate.edu/Thesis/McMeeking%20dissertation.pdf

Mischenko, M. I., Travis, L. D., and Lacis, A. A.: Scattering, Absorption, and Emission of Light by Small Particles, Cambridge University Press, UK, 2002.

Moise, T., Flores, J. M., and Rudich, Y.: Optical Properties of Secondary Organic Aerosols and Their Changes by Chemical Processes, Chemical reviews, 115, 4400-4439, 2015.

Murphy, B. N. and Pandis, S. N.: Exploring summertime organic aerosol formation in the eastern United States using a regional-scale budget approach and ambient measurements, Journal of Geophysical Research, 115, 2010.

Myhre, G., Samset, B., Schulz, M., Balkanski, Y., Bauer, S., Berntsen, T., Bian, H., Bellouin, N., Chin, M., and Diehl, T.: Radiative forcing of the direct aerosol effect from AeroCom Phase II simulations, Atmospheric Chemistry and Physics, 13, 1853-1877, 2013.

Nakayama, T., Matsumi, Y., Sato, K., Imamura, T., Yamazaki, A., and Uchiyama, A.: Laboratory studies on optical properties of secondary organic aerosols generated during the photooxidation of toluene and the ozonolysis of α-pinene, Journal of Geophysical Research, 115, D24204, 2010.

Nakayama, T., Sato, K., Matsumi, Y., Imamura, T., Yamazaki, A., and Uchiyama, A.: Wavelength and NO x dependent complex refractive index of SOAs generated from the photooxidation of toluene, Atmospheric Chemistry and Physics, 13, 531-545, 2013.

Nguyen, T. B., Lee, P. B., Updyke, K. M., Bones, D. L., Laskin, J., Laskin, A., and Nizkorodov, S. A.: Formation of nitrogen-and sulfur-containing light-absorbing compounds accelerated by evaporation of water from secondary organic aerosols, Journal of Geophysical Research, 117, 01207, 2012.

Park, R. J., Jacob, D. J., Chin, M., and Martin, R. V.: Sources of carbonaceous aerosols over the United States and implications for natural visibility, Journal of Geophysical Research, 108, 4355, 2003.

Park, R. J., Jacob, D. J., Kumar, N., and Yantosca, R. M.: Regional visibility statistics in the United States: Natural and transboundary pollution influences, and implications for the Regional Haze Rule, Atmospheric Environment, 40, 5405-5423, 2006.

Park, R. J., Kim, M. J., Jeong, J. I., Youn, D., and Kim, S.: A contribution of brown carbon

947 aerosol to the aerosol light absorption and its radiative forcing in East Asia, Atmospheric
948 Environment, 44, 1414-1421, 2010.

949 Reid, J., Koppmann, R., Eck, T., and Eleuterio, D.: A review of biomass burning emissions
950 part II: intensive physical properties of biomass burning particles, Atmospheric Chemistry
951 and Physics, 5, 799-825, 2005.

952 Rienecker, M. M., Suarez, M. J., Gelaro, R., Todling, R., Bacmeister, J., Liu, E., Bosilovich,
953 M. G., Schubert, S. D., Takacs, L., and Kim, G.-K.: MERRA: NASA's modern-era
954 retrospective analysis for research and applications, Journal of Climate, 24, 3624-3648, 2011.

955 Saleh, R., Robinson, E. S., Tkacik, D. S., Ahern, A. T., Liu, S., Aiken, A. C., Sullivan, R. C.,
956 Presto, A. A., Dubey, M. K., and Yokelson, R. J.: Brownness of organics in aerosols from
957 biomass burning linked to their black carbon content, Nature Geoscience, 7, 647-650, 2014.

958 Schnaiter, M., Gimmler, M., Llamas, I., Linke, C., Jäger, C., and Mutschke, H.: Strong
959 spectral dependence of light absorption by organic carbon particles formed by propane
960 combustion, Atmospheric Chemistry and Physics, 6, 2981-2990, 2006.

961 Srinivas, B. and Sarin, M.: Brown carbon in atmospheric outflow from the Indo-Gangetic
962 Plain: Mass absorption efficiency and temporal variability, Atmospheric Environment, 89,
963 835-843, 2014.

964 Turpin, B. J. and Lim, H. J.: Species contributions to PM2. 5 mass concentrations: Revisiting
965 common assumptions for estimating organic mass, Aerosol Science & Technology, 35, 602-
966 610, 2001.

967 Updyke, K. M., Nguyen, T. B., and Nizkorodov, S. A.: Formation of Brown Carbon via
968 Reactions of Ammonia with Secondary Organic Aerosols from Biogenic and Anthropogenic
969 Precursors, Atmospheric Environment, 63, 22-31, 2012.

970 Wang, X., Heald, C., Ridley, D., Schwarz, J., Spackman, J., Perring, A., Coe, H., Liu, D., and
971 Clarke, A.: Exploiting simultaneous observational constraints on mass and absorption to
972 estimate the global direct radiative forcing of black carbon and brown carbon, Atmospheric
973 Chemistry and Physics, 14, 10989-11010, 2014.

974 Ward, D., Susott, R., Kauffman, J., Babbitt, R., Cummings, D., Dias, B., Holben, B.,
975 Kaufman, Y., Rasmussen, R., and Setzer, A.: Smoke and Fire Characteristics for Cerrado and

976 Deforestation Burns in Brazil: BASE-B Experiment, Journal of Geophysical Research, 97,
977 14601-14619, 1992.

978 Ward, D. E. and Hao, W.: Projections of Emissions from Burning of Biomass Foruse in
979 Studies of Global Climate and Atmospheric Chemistry, Air and Waste Management
980 Association, Vancouver, British Colombia, Canada, 1991.

981 Weber, R. J., Sullivan, A. P., Peltier, R. E., Russell, A., Yan, B., Zheng, M., de Gouw, J.,
982 Warneke, C., Brock, C., and Holloway, J. S.: A study of secondary organic aerosol formation
983 in the anthropogenic-influenced southeastern United States, Journal of Geophysical Research,
984 112, D13302, 2007.

985 Wiedinmyer, C., Akagi, S., Yokelson, R., Emmons, L., Al-Saadi, J., Orlando, J., and Soja, A.:
986 The Fire INventory from NCAR (FINN): a high resolution global model to estimate the
987 emissions from open burning, Geoscientific Model Development, 4, 625-641, 2011.

988 Yang, M., Howell, S., Zhuang, J., and Huebert, B.: Attribution of aerosol light absorption to
989 black carbon, brown carbon, and dust in China–interpretations of atmospheric measurements
990 during EAST-AIRE, Atmospheric Chemistry and Physics, 9, 2035-2050, 2009.

991 Yu, L., Smith, J., Laskin, A., Anastasio, C., Laskin, J., and Zhang, Q.: Chemical
992 characterization of SOA formed from aqueous-phase reactions of phenols with the triplet
993 excited state of carbonyl and hydroxyl radical, Atmospheric Chemistry and Physics, 14,
994 13801-13816, 2014.

995 Zhang, X., Lin, Y.-H., Surratt, J. D., and Weber, R. J.: Sources, Composition and Absorption
996 Ångström Exponent of Light-absorbing Organic Components in Aerosol Extracts from the
997 Los Angeles Basin, Environmental Science & Technology, doi: 10.1021/es305047b, 2013.
998 2013.

999 Zhang, X., Lin, Y. H., Surratt, J. D., Zotter, P., Prévôt, A. S. H., and Weber, R. J.: Light-
1000 absorbing soluble organic aerosol in Los Angeles and Atlanta: A contrast in secondary
1001 organic aerosol, Geophysical Research Letters, 38, 21810, 2011.

1002 Zhong, M. and Jang, M.: Light absorption coefficient measurement of SOA using a UV-
1003 Visible spectrometer connected with an integrating sphere, Atmospheric Environment, 45,
1004 4263-4271, 2011.

Zhong, M., Jang, M., Oliferenko, A., Pillai, G. G., and Katritzky, A. R.: The SOA Formation Model Combined with Semiempirical Quantum Chemistry to Predict UV-Vis Absorption of Secondary Organic Aerosols, Physial Chemistry Chemical Physics, 14, 9058-9066, 2012.

Table 1. Emission factors (EFs) and calculated parameters used for primary BrC emission estimates. Biomass burning emission is classified for six vegetation types based on the FINN inventory. Here BrC/OC is the mass ratio of BrC to OC emitted from biomass burning and biofuel use.

Source Type	**CO_2 EF [g kg^{-1}]**	**CO EF [g kg^{-1}]**	**MCE**	**OC EF [g kg^{-1}]**	**BC EF [g kg^{-1}]**	**BrC/OC**		
Biomass burning						case1	case2	case3
Boreal Forest	1514	118	0.891	7.8	0.20	0.135	0.093	0.057
Cropland	1537	111	0.898	3.3	0.69	0.946	0.652	0.400
Savanna/Grassland	1692	59	0.948	2.6	0.37	0.189	0.123	0.067
Temperate Forest	1630	102	0.910	9.2	0.56	0.211	0.145	0.088
Tropical Forest	1643	92	0.919	4.7	0.52	0.312	0.213	0.128
Woody Savannah/Shrubland	1716	68	0.941	6.6	0.50	0.123	0.081	0.046
Biofuel[1)]						0.663	0.452	0.271

1) Detailed information is given in Table 2

Table 2. Global biofuel consumption estimates, EFs of OC, and OC biofuel emission estimates for each biofuel category. Base year is 2000.

		Fuelwood	Crop Residues	Dung	Charcoal	Industrial	Total
Biofuel Consumption[1] [Tg]		1351	495	75	39	498	2457
EF [g/kg][2]		2.97[3]	3.3	1.8	1.3	0.91[3]	2.6
OC emission [Gg]		4010.3	1633.5	135	50.7	453.6	6281[4]
BrC/OC	case1	0.653	0.946	0.000	0.000	0.000	
	case2	0.442	0.652	0.000	0.000	0.000	
	case3	0.261	0.400	0.000	0.000	0.000	

1) From Fernandes et al. (2007)
2) From Bond et al. (2004)
3) Global mean value is estimated from Bond et al. (2004)
4) From GEOS-Chem biofuel OC inventory (carbon_200909) by Bond et al. (2007)

Table 3. Global tropospheric budgets of BrC compared to those of OC and BC. Uncertainties are indicated in the parentheses.

Unit : [GgC]	BrC			OC	BC	BrC/OC	BrC/BC
Sources	Biomass burning	3857	(±1689)				
	Biofuel	2965	(±1281)			0.27	1.83
	Anthropogenic SOC	5690				(±0.06)	(±0.43)
	Total	12512	(±2970)	46929	6847		
Wet Deposition	Biomass burning	3169	(±1389)				
	Biofuel	2358	(±1018)			0.28	1.97
	Anthropogenic SOC	5244				(±0.07)	(±0.45)
	Total	10771	(±2407)	38681	5458		
Dry Deposition	Biomass burning	688	(±301)				
	Biofuel	607	(±263)			0.21	1.25
	Anthropogenic SOC	445				(±0.07)	(±0.41)
	Total	1740	(±564)	8272	1397		
Burden	Biomass burning	59	(±26)				
	Biofuel	40	(±18)			0.19	1.84
	Anthropogenic SOC	98				(±0.05)	(±0.41)
	Total	197	(±44)	1021	107		
Lifetime [days]	Biomass burning	5.6	(±0.0)				
	Biofuel	5.0	(±0.0)				
	Anthropogenic SOC	6.3					
	Total	5.8	(±0.1)	7.9	5.7		

Table 4. Extinction efficiencies and SSAs of selected aerosols at 0.4 μm used for calculating photolysis rates in GEOS-Chem. SNA indicates inorganic salt comprised of sulfate, nitrate and ammonium aerosols.

0.4 μm	RH	BrC (Primary)	BrC (Secondary)	OC	BC	SNA
Extinction Efficiency	0%	1.4644	1.2922	1.3933	0.6229	1.2147
	50%	1.6995	1.5645	1.4967	0.6229	1.6566
	70%	1.7873	1.6781	1.5815	0.6229	1.8440
	90%	1.8386	1.7474	1.8485	0.4607	2.2568
	99%	2.2696	2.4390	2.5870	0.4181	2.9655
Single Scattering Albedo	0%	0.5621	0.8683	0.9735	0.1935	1.0000
	50%	0.5474	0.8584	0.9841	0.1935	1.0000
	70%	0.5422	0.8540	0.9873	0.1935	1.0000
	90%	0.5342	0.8480	0.9927	0.3004	1.0000
	99%	0.5412	0.8372	0.9977	0.5233	1.0000

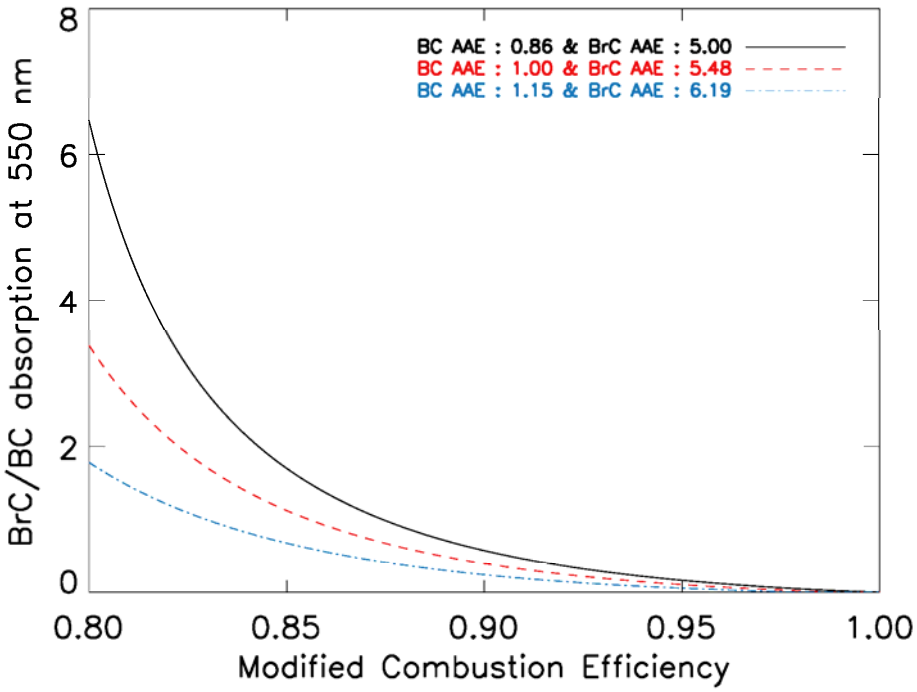

Figure 1. Estimated absorption ratios of BrC to BC at 550 nm as a function of MCE. We assume that the CA absorption is only contributed by BC and BrC absorption. Black solid line indicates case 1, red dashed line represents case 2, and blue dotted line shows case 3.

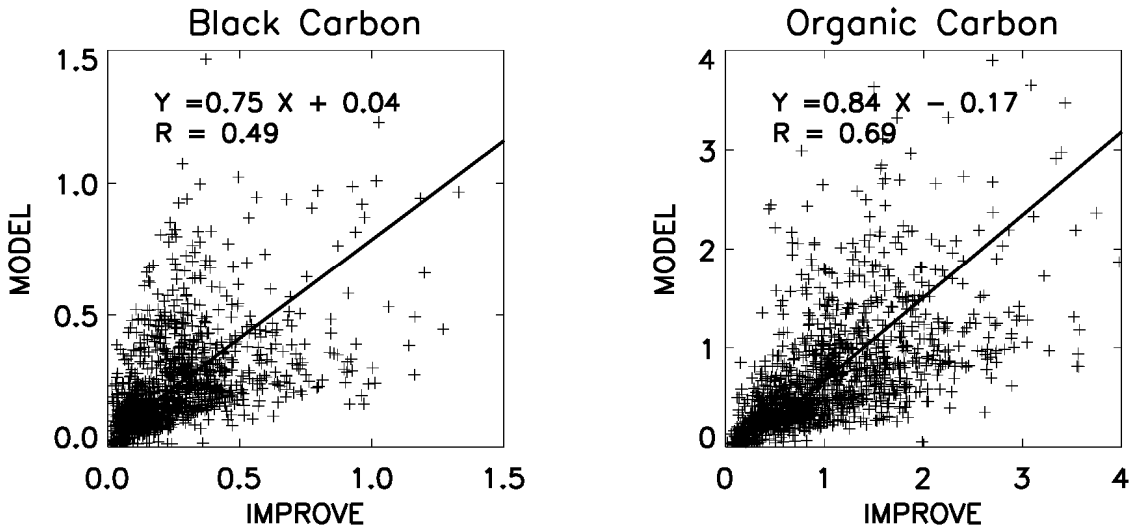

Figure 2. Scatterplot of simulated versus observed BC concentrations (left) and OC concentrations (right). Unit is μgC m^{-3}. Values are monthly means for 2007. Regression equations and correlations are shown inset. Regression is computed with reduced major axis (RMA) method.

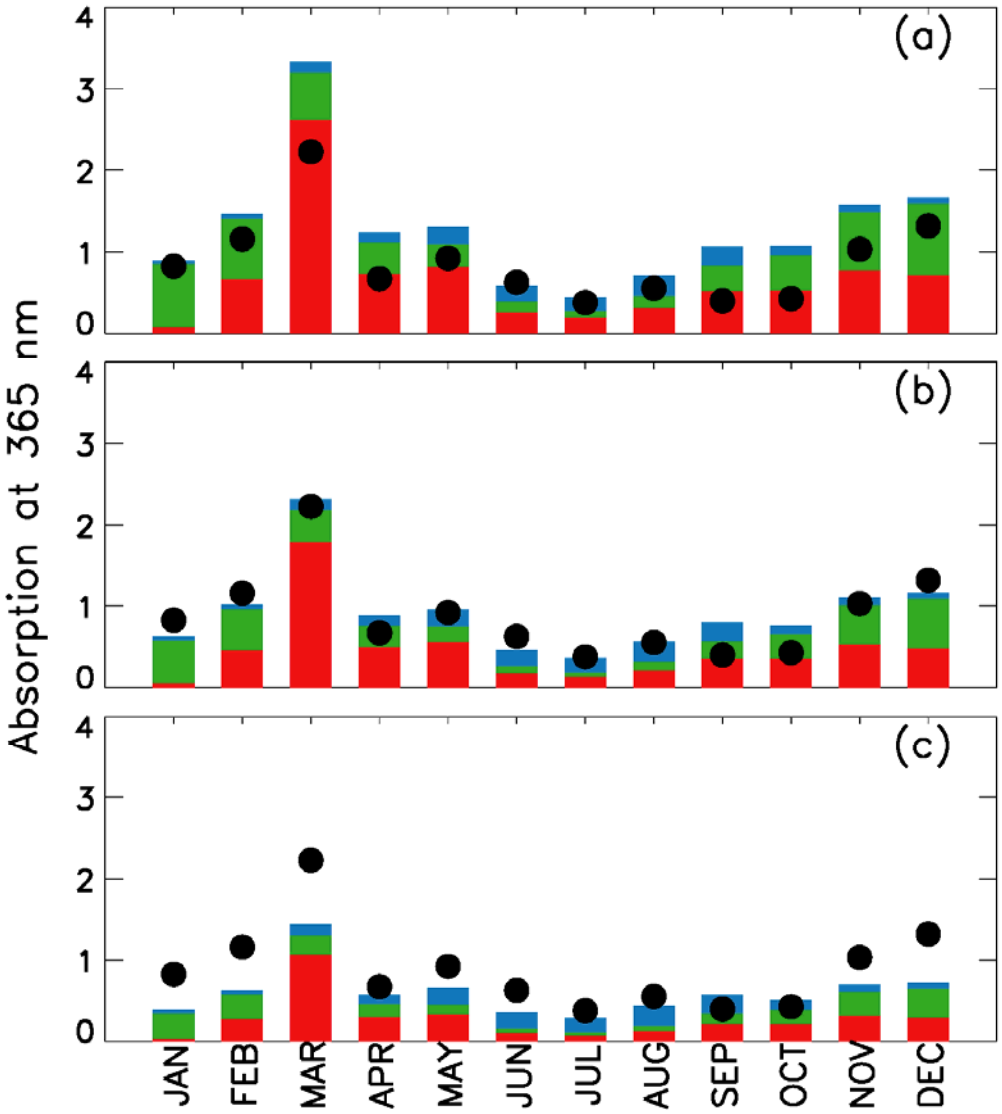

Figure 3. Simulated versus observed monthly mean light absorption at 365 nm by water soluble BrC over the southeastern US in 2007. Unit is Mm^{-1}. Black circles denote observations, and bar graphs indicate model results for each source: biomass burning (red), biofuel (green), and SOA (blue). Each panel shows the comparisons with different emission estimate cases – (a) case 1, (b) case 2, and (c) case 3.

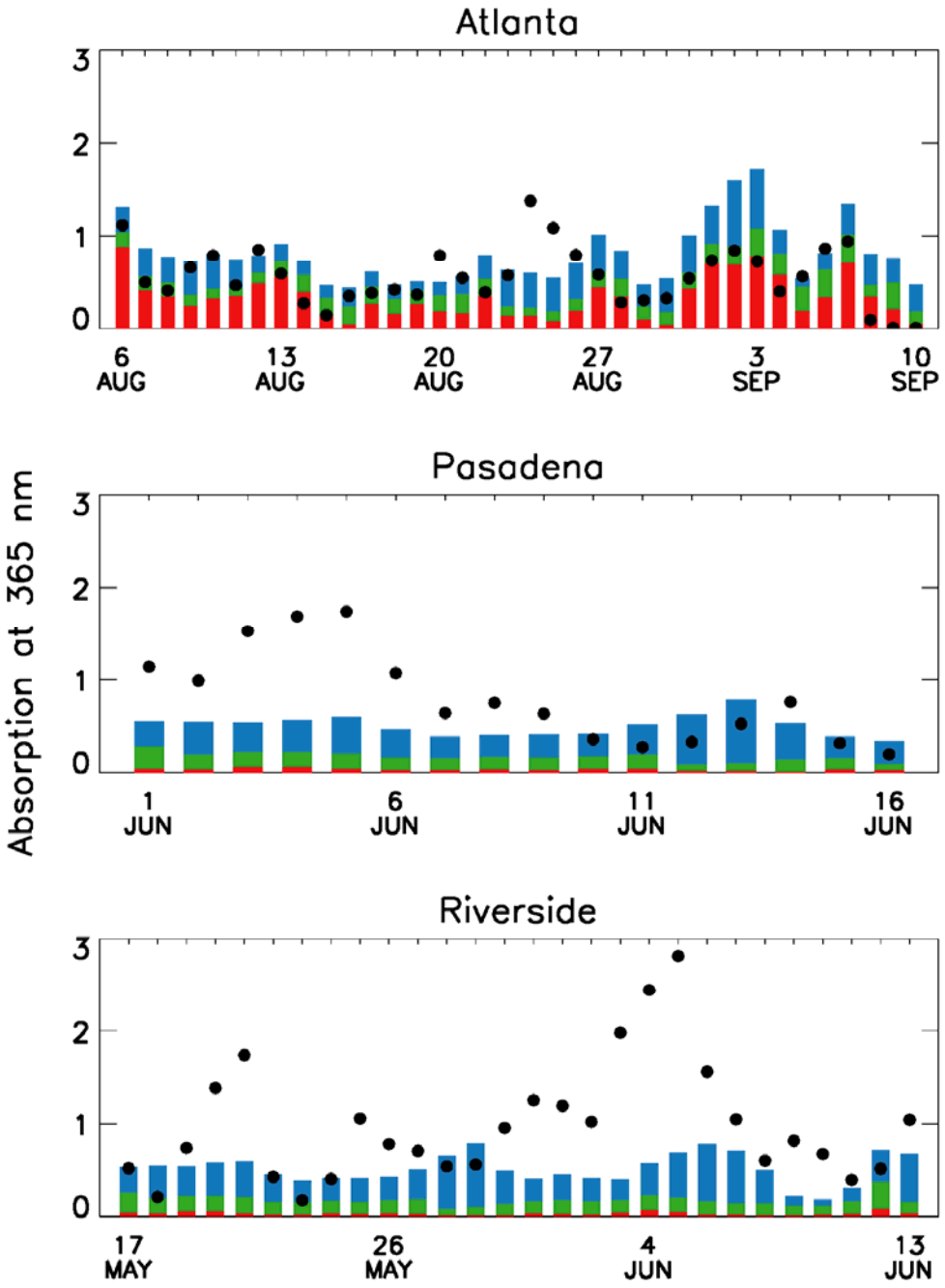

Figure 4. Simulated versus observed daily mean light absorption at 365 nm by water soluble BrC over the US in 2010. Unit is Mm^{-1}. Black circles denote observations and bar graphs indicate model results for each source – biomass burning (red), biofuel (green), and SOA (blue).

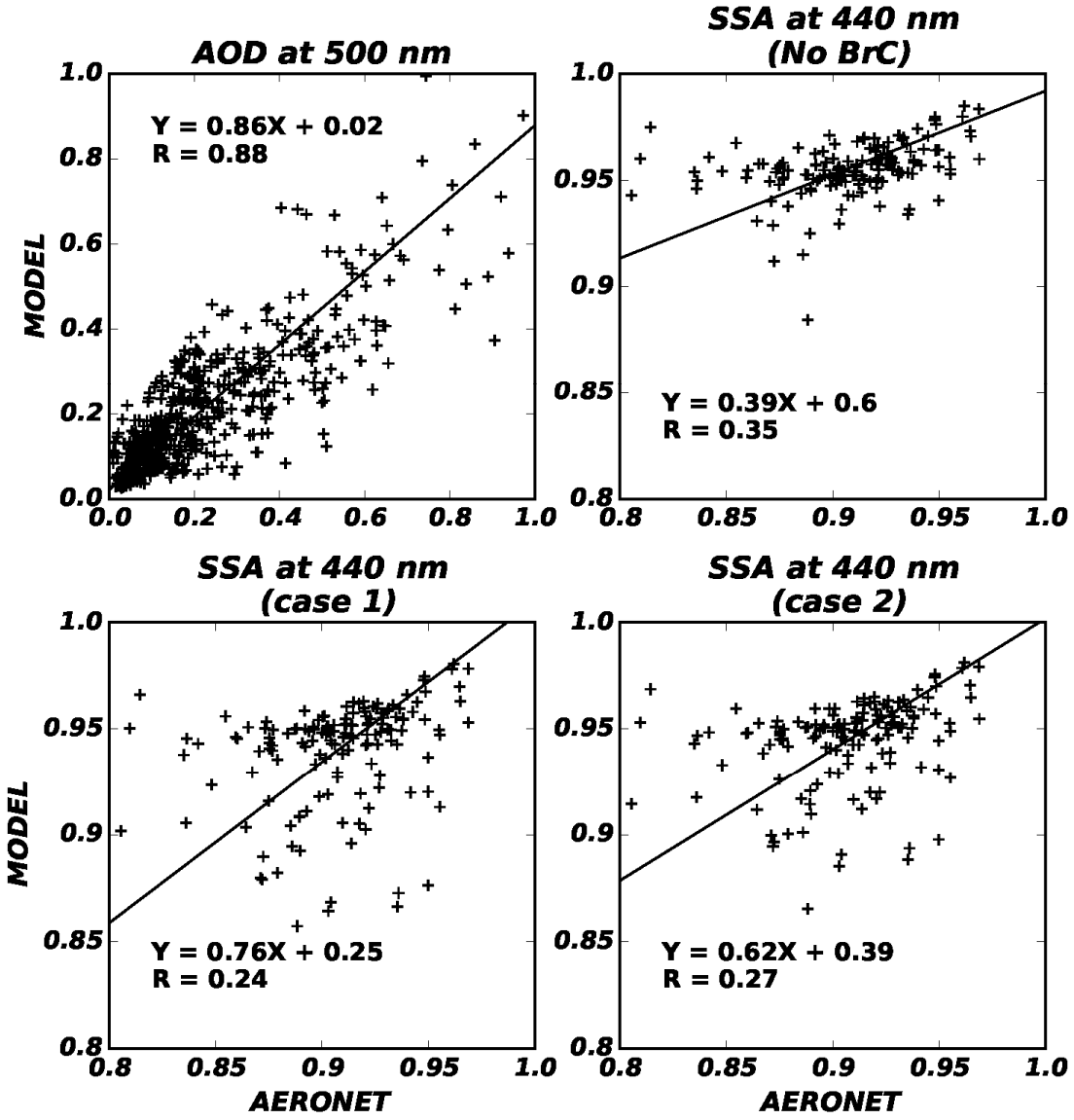

Figure 5. Scatterplots of simulated versus observed AOD at 500 nm (upper left), SSA at 440 nm without BrC (upper right), SSA at 440 nm with BrC of case 1 (lower left), and SSA at 440 nm with BrC of case 2 (lower right) for 2007. Reduced major axis regression is shown along with the regression equation and R. Each point indicates monthly averaged AOD or SSA when the number of observation is greater than 10 days.

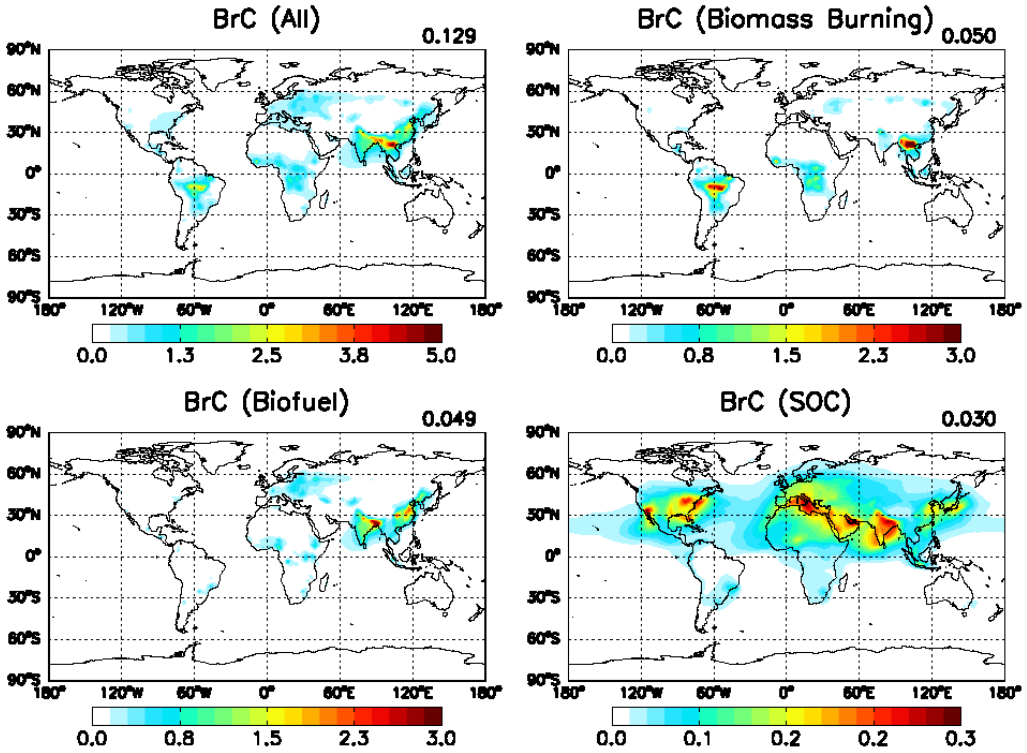

Figure 6. Annual surface map of total BrC (top left) and BrC from three source categories: biomass burning (top right), biofuel (bottom left), and SOC (bottom right). Mean values are presented in the upper right corner of each panel. Unit is μgC m^{-3}.

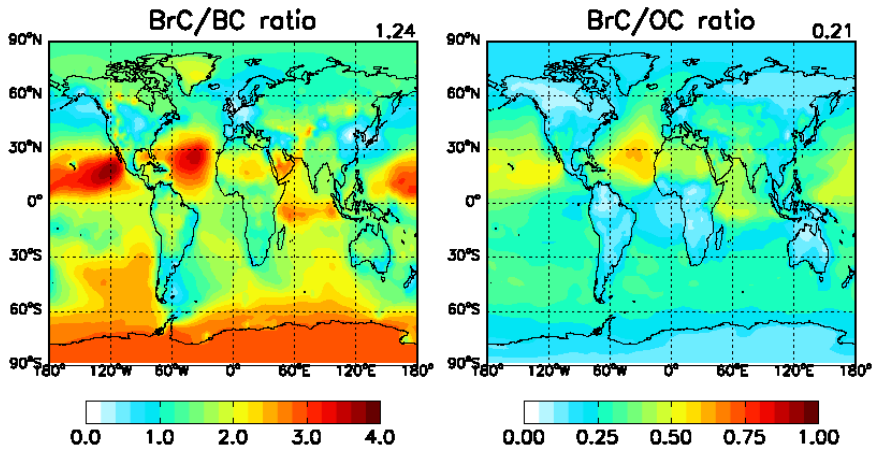

Figure 7. Annual mean ratios of BrC to BC (left) and OC (right) in surface air. Global mean values are presented in the upper right corner of each panel.

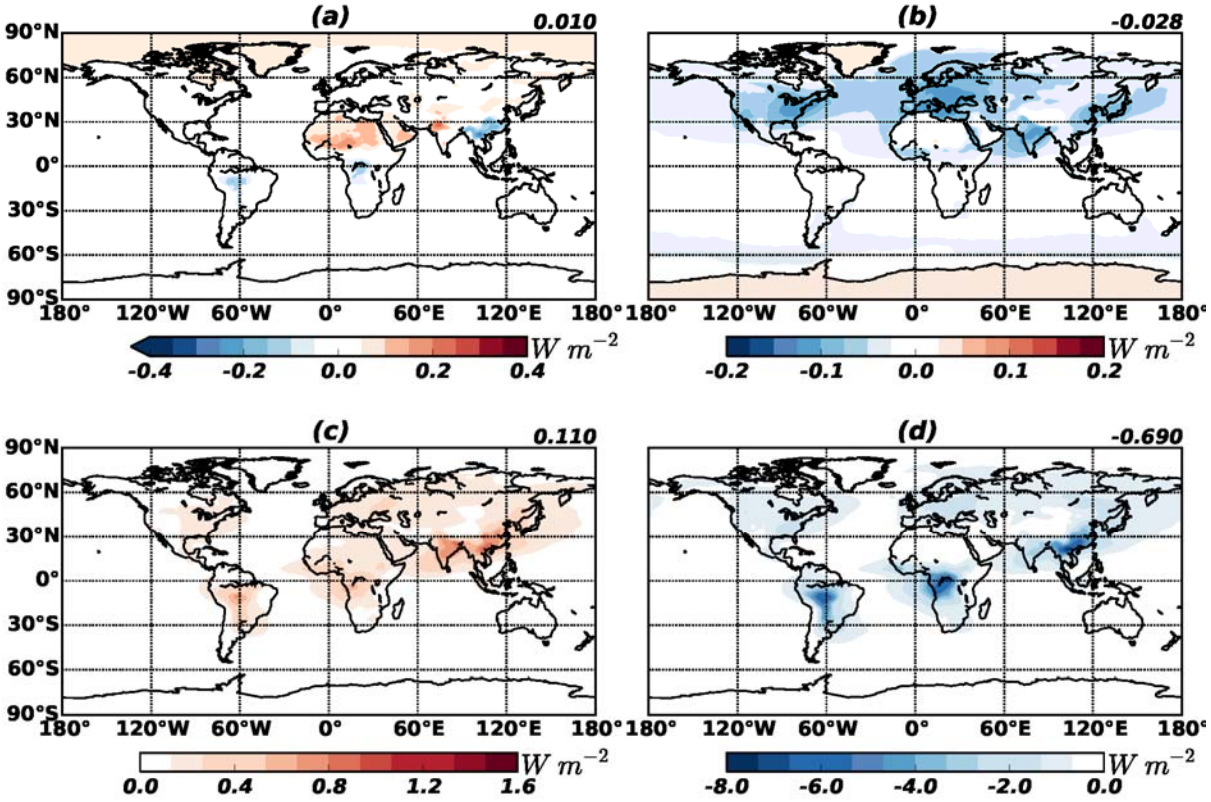

Figure 8. DRE of BrC at the top of the atmosphere. Upper panels are for radiative effect of BrC from primary sources (a) and from secondary sources (b). The DRE increase of OC owing to the absorption of BrC is shown in (c) (i.e. the DRE of OC with absorbing BrC minus the DRE of OC including BrC as scattering OC, which is typically assumed in previous studies). Radiative effect of total OC (BrC is assumed to be scattering OC) is represented in (d). The 70°S–70°N averages are shown in the upper right corner of each panel.

1175

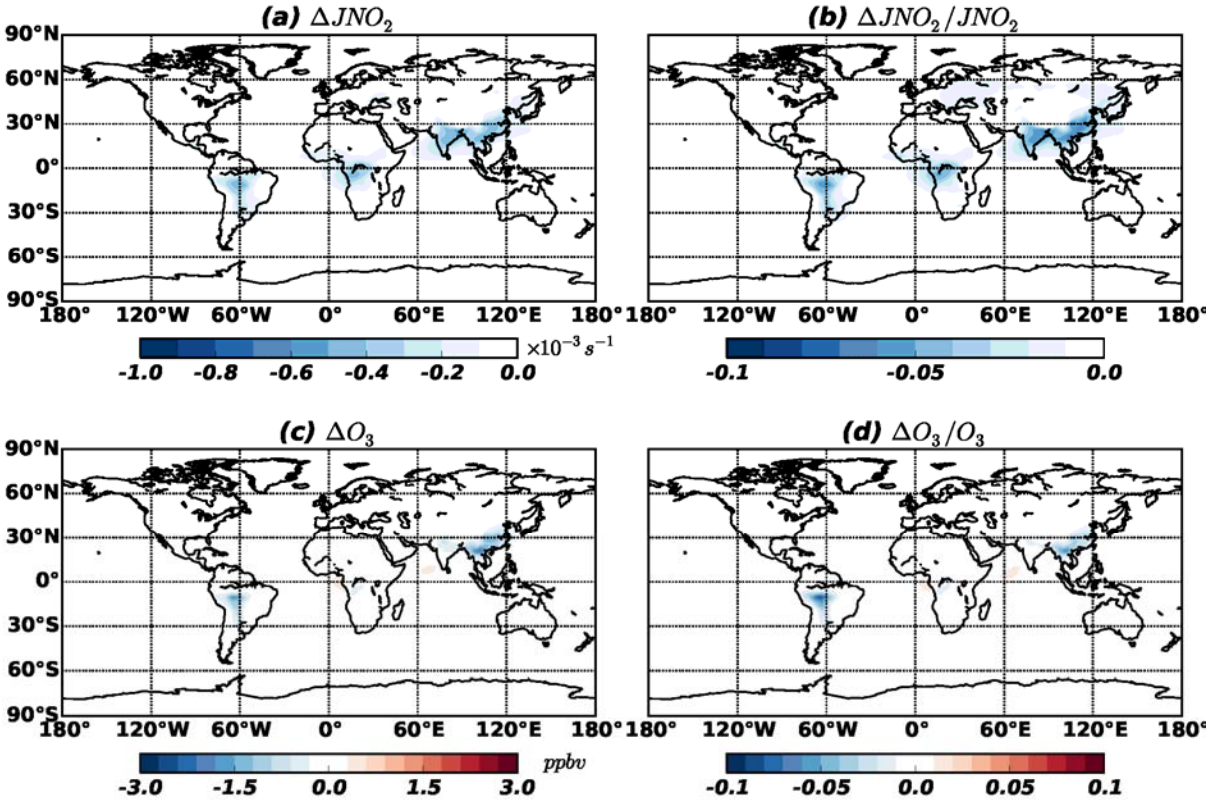

1176

1177 Figure 9. Changes in annual NO_2 photolysis rate (a,b) and O_3 concentration (c,d) at the surface
1178 due to BrC absorption.

1179

1180

1181